Influence of Capillary Barrier Effect on Biogas Distribution at the Base of Passive Methane Oxidation Biosystems: Parametric Study

Bahar Ahoughalandari [a] and Alexandre R. Cabral [a,*]

[a] Geoenvironmental Group, Department of Civil Engineering, University of Sherbrooke, Sherbrooke, Quebec, Canada J1K 2R1.

*Corresponding author: Tel.: +1 819 821-7906. Postal address: 2500, boul. de l'Université, Sherbrooke, Quebec, Canada J1K 2R1.

E-mail addresses: alexandre.cabral@usherbrooke.ca (A. R. Cabral); bahar.ahou@usherbrooke.ca (B. Ahoughalandari)

Waste Management 63 (2017) 172–187

ARTICLE INFO

Article history:
Received 12 May 2016
Revised 17 November 2016
Accepted 18 November 2016
Available online 5 December 2016

Keywords:
Landfill final covers
Passive methane oxidation
Biogas flow behavior
Capillary barrier effect
Numerical simulation

* Corresponding author at: 2500, boul. de l'Université, Sherbrooke, Quebec J1K 2R1, Canada
E-mail addresses: bahar.ahou@usherbrooke.ca (B. Ahoughalandari), alexandre.cabral@usherbrooke.ca (A.R. Cabral).

Abstract

The efficiency of methane oxidation in passive methane oxidation biosystems (PMOBs) is influenced by, among other things, the intensity and distribution of the CH_4 loading at the base of the methane oxidation layer (MOL). Both the intensity and distribution are affected by the capillary barrier that results from the superposition of the two materials constituting the PMOB, namely the MOL and the gas distribution layer (GDL). The effect of capillary barriers on the unsaturated flow of water has been well documented in the literature. However, its effect on gas flow through PMOBs is still poorly documented. In this study, sets of numerical simulations were performed to evaluate the effect of unsaturated hydraulic characteristics of the MOL material on the value and distribution of moisture and hence, the ease and uniformity in the distribution of the upward flow of biogas along the GDL-MOL interface. The unsaturated hydraulic parameters of the materials used to construct the experimental field plot at the St-Nicephore landfill (Quebec, Canada) were adopted to build the reference simulation of the parametric study. The behavior of the upward flow of biogas for this particular material was analyzed based on its gas intrinsic permeability function, which was obtained in the laboratory. The parameters that most influenced the distribution and the ease of biogas flow at the base of the MOL were the saturated hydraulic conductivity and pore size distribution of the MOL material, whose effects were intensified as the slope of the interface increased. The effect of initial dry density was also assessed herein. Selection of the MOL material must be made bearing in mind that these three parameters are key in the effort to prevent unwanted restriction in the upward flow of biogas, which may result in the redirection of biogas towards the top of the slope, leading to high CH_4 fluxes (hotspots). In a well-designed PMOB, upward flow of biogas across the GDL-MOL interface is unrestricted and moisture distribution is uniform. This paper tries to show how to obtain this.

Keywords: Landfill final covers; Passive methane oxidation; Biogas flow behavior; Capillary barrier effect; Numerical simulation

Glossary

PMOB: passive methane oxidation biosystems

MOL: methane oxidation layer

GDL: gas distribution layer

LUGM: length of unrestricted gas migration

θ_w: volumetric water content

$\Delta\theta_w$: difference between maximum and minimum values of volumetric water content along the interface

θ_a: volumetric air content

$\theta_{a\text{-}occ}$: occlusion value

$\theta_{a\text{-}pocc}$: pre-occlusion value

$\theta_{w\text{-}occ}$: volumetric water content associated with occlusion value

$\theta_{w\text{-}pocc}$: volumetric water content associated with pre-occlusion value

$\theta_{w\text{-}max}$: maximum value of volumetric water content along the interface

a: curve fitting parameter for the van Genuchten (1980) model

n: curve fitting parameter for the van Genuchten (1980) model

$k_{sat\text{-}MOL}$: saturated hydraulic conductivity of methane oxidation layer material

1. Introduction

A capillary barrier is formed when water flows through two superimposed soil layers with contrasting unsaturated hydraulic properties. Capillary forces associated with this contrast create a capillary block along the interface, which limits vertical percolation of water through the interface and reduces gas fluxes, and in the case of inclined capillary barriers, may laterally drain the meteoric seepage.

Capillary barriers are often incorporated into the design of final covers for landfills, acid-generating mine tailings and waste-rock dumps. In the case of landfills, the design of the final cover must consider maximum seepage rates imposed by legislation to control the infiltration, therefore leachate generation (e.g. Aubertin et al. 2006; Bussière et al. 2003a; Khire et al. 2000; Stormont 1996; Vachon et al. 2015). In the case of mine residues, the goal is to prevent the influx of atmospheric oxygen, thereby preventing the generation of acid mine drainage (Adu-Wusu and Yanful 2006; Bussière et al. 2003b; Dagenais et al. 2005; Williams et al. 1997; Wilson et al. 1995; Yanful 1993).

Recently, passive methane oxidation biosystems (PMOBs) have been promoted as a means of reducing fugitive CH_4 emissions (emissions not captured by gas collection systems) from landfills. PMOBs are of particular importance during the aftercare phase, i.e. following the shutdown of active gas collection (e.g. Cabral et al. 2010b; Huber-Humer et al. 2009; Roncato and Cabral 2012; Sadasivam and Reddy 2014).

PMOBs are engineered systems installed at the top-most part of the final cover and consist of two main layers: the methane oxidation layer (MOL), localized near the surface and where most CH_4 is oxidized into CO_2 (using atmospheric O_2) by methanotrophic bacteria, and the underlying gas distribution layer (GDL), which intercepts fugitive emissions. The methane oxidation efficiency of PMOBs depends on several parameters, including the CH_4 loading at

85 the base of the PMOB (Cabral et al. 2010b; Fredenslund et al. 2010; Gebert et al. 2011;
86 Ndanga et al. 2015; Pokhrel et al. 2011; Rachor et al. 2011; Scheutz et al. 2011). The lower
87 the CH_4 loading, the more the methanotrophs will be capable of oxidizing the upward flow of
88 biogas intercepted by the gas distribution layer. To reduce the loading, this upward flow has
89 to be distributed over the widest surface possible.

90 The contrast in unsaturated hydraulic behavior between the materials of the methane
91 oxidation layer and the gas distribution layer results in capillary barrier formation along the
92 interface (AhouGhalandari et al. 2015; Tétreault et al. 2013). As a result, the methane
93 oxidation layer retains water and, therefore, its degree of saturation increases where the
94 capillary block occurs, i.e. along the GDL-MOL interface. In an inclined interface, the
95 retained water seeps both laterally and vertically, causing an increase in the degree of
96 saturation towards the bottom of the slope. The ensuing effects of the degree of saturation on
97 occlusion of air-filled pores and gas flow has been the object of several studies dealing with
98 unsaturated flow through porous media (e.g. Jucá and Maciel 2006; Langfelder et al. 1968;
99 Maciel and Jucá 2000; Marinho et al. 2001). Beyond a certain point along the sloping
100 interface, the increase in the degree of saturation may lead to occlusion of air-filled pores,
101 and therefore restrict the upward flow of biogas. As a consequence, biogas diverts toward the
102 regions of the biosystem with lower degrees of saturation located upstream (Tétreault et al.
103 2013). This may in turn create a hotspot, i.e. a localized region where surface CH_4
104 concentrations are higher than acceptable by legislation and where methane oxidation is
105 much lower (Bohn and Jager 2009; Cabral et al. 2010a; Röwer et al. 2012).

106 It stems from the preceding that an efficient PMOB design would be associated with the
107 longest possible length along the GDL-MOL interface where upward gas migration is
108 unrestricted. This length is herein denominated *length of unrestricted gas migration*
109 (LUGM).

Bohn and Jager (2009) observed the persistent presence of a hotspot upslope a large-scale experimental PMOB constructed in Germany, with a slope of 1V:10H. Similarly, the surface emission measurements performed by Röwer et al. (2012) and Geck et al. (2012) showed upslope hotspots in an experimental PMOB with a slope of 1V:5H, constructed in the Netherlands. Both PMOBs were composed of a two-material recultivation layer (protection and vegetation layers) as the methane oxidation layer, and a two-layer capillary barrier that was constructed to control infiltration, but that also acted as the gas distribution layer. Conducting a series of steady-state numerical simulations on these two PMOBs, Tétreault et al. (2013) concluded that biogas could flow unrestricted through the gas distribution layers, where the degrees of saturation were low, but pore occlusion likely occurred at the GDL-MOL interfaces. Hotspots upstream of the PMOBs most probably resulted from pore occlusion. Kjeldsen et al. (2013) constructed an experimental PMOB with a jagged GDL-MOL interface with the intention of limiting potential pore occlusion (resulting from accumulation of moisture along the interface) to the lower parts of each segment. Moisture along the interface in the upper part of each segment would be low enough, thereby allowing the CH_4 loading to seep freely into the methane oxidation layer.

This very ingenious idea put forth by Kjeldsen et al. (2013) needs to be further developed, in order to incorporate proper design steps and parameters. Indeed, there seems to be a need for more rigorous numerical studies on gas flow behavior through PMOBs that includes consideration of the capillary barrier effect and the importance of uniformity of biogas distribution and the ease of upward biogas flow. Such studies would provide tools for selecting materials for the methane oxidation and gas distribution layers with appropriate geotechnical and hydraulic characteristics and geometrical parameters of PMOBs.

The focus of this study was to evaluate how the distribution of biogas along the interface of an inclined PMOB was affected by the slope of the PMOB, and by some of the basic

unsaturated hydraulic parameters of MOL material. A parametric study was conducted using data from an experimental PMOB constructed at the St-Nicephore landfill as a starting point (or *Reference simulation*). Several years of monitoring this PMOB have shown it to be a highly efficient PMOB, capable of oxidizing very high CH_4 loads (Capanema and Cabral 2012; Roncato and Cabral 2012).

Transient state numerical simulations were performed using the commercial program SEEP/W (2010). As previously mentioned, the main variables in these simulations included the slope of the GDL-MOL interface and the unsaturated hydraulic properties of the MOL material, i.e. the water retention curve and saturated hydraulic conductivity. The simulations made it possible to evaluate the effect of each variable on the distribution of moisture along the GDL-MOL interface and the magnitude of LUGM.

The tools proposed herein are another necessary step in the development of PMOB design. The study is innovative insofar as it brings the hydraulic aspects and unsaturated flow to the forefront of PMOB design, which have not yet received the attention they deserve. The main limitations of the study are two-fold. The first is related to the lack of consideration of evapotranspiration in the numerical simulations, and, indirectly, to the importance of plant roots or vegetation in moisture release or retention. This limitation was circumvented by considering that a reasonable percentage of the total precipitation actually seeped through the cover and reached the GDL-MOL interface. The second limitation relates to the lack of consideration of water generation during biotic activities in the numerical simulations presented herein. This would most certainly be an important addition to a proper design.

2. Materials and methods

2.1. Site configuration

The experimental PMOB numerically analyzed in this study is one of the three PMOBs constructed within the existing final cover of the St-Nicephore landfill, Quebec, Canada to evaluate the methane oxidation efficiency of the designs under field conditions (Capanema and Cabral 2012; Roncato and Cabral 2012). This PMOB, referred to in the literature as PMOB2, measured 2.75 m (W) × 9.75 m (L) with a slope of 3.5%. A drainage system was installed at the lowest point to evacuate percolated water. It consisted of an 80-cm-thick methane oxidation layer containing a mixture of five volumes of compost and one volume of coarse sand. The main characteristics of the sand-compost mixture were the following: specific gravity (G_s) = 2.24, $S_{r\text{-}opt}$ (degree of saturation at line of optima) = 90%, $\rho_{d\text{-}insitu}$ (in situ dry density) = 750 kg/m^3, in situ porosity equal to 0.665 and in situ gravimetric water content on the day of field measurements (w%) = 47% (taken at mid-depth and mid-length of the MOL). These values were used as initial conditions in numerical simulations. The MOL material of PMOB2 (experimental field plot at the St-Nicephore landfill) is denominated herein as *Reference MOL*. The 40-cm-thick gas distribution layer was constructed using 12.7-mm clean gravel, which was placed under the methane oxidation layer.

2.2. Hydraulic properties of the materials

The drying water retention curve of the *Reference MOL* was determined using the HYPROP apparatus (HYPROP-UMS 2013), at in situ initial dry density and water content (AhouGhalandari et al. 2015). For the gas distribution layer, the water retention curve was estimated using the Fredlund et al. model (Fredlund et al. 2002), derived from the grain size distribution curve of the material. In the present study, the effect of hysteresis of the water retention curve was not considered and only the drying curve was used. Saturated hydraulic conductivity (k_{sat}) of the *Reference MOL* was equal to 9×10^{-6} m/s, which was measured

183 according to ASTM D2434-68 (ASTM-D2434-68 2006) at in situ initial dry density and
184 water content. The k_{sat} of the gas distribution layer material was calculated using the Chapuis
185 equation (2004).

186 The van Genuchten model (1980) was used to fit the water retention curve (Equation 1),
187 whereas hydraulic conductivity functions were obtained using the van Genuchten model
188 (1980), based on the Mualem formulation (1976) (Equation 2). The water retention curve and
189 hydraulic conductivity functions obtained were then used during the simulations using
190 SEEP/W (Figure 1 and Figure 2).

191

192 $$\theta_w = \theta_r + \frac{\theta_s - \theta_r}{\left[1 + \left(\frac{\psi}{a}\right)^n\right]^m} \quad (1)$$

193 $$k_w = k_{sat} \frac{\left[1 - \left(a\psi^{(n-1)}\right)\left(1 + \left(a\psi^n\right)^{-m}\right)\right]^2}{\left[\left((1 + a\psi)^n\right)^{\frac{m}{2}}\right]} \quad (2)$$

194

195 where k_w is the hydraulic conductivity, θ_w is volumetric water content, θ_s is saturated
196 volumetric water content, θ_r is residual volumetric water content, ψ is suction, *a* is related to
197 the inverse of the air entry value, *n* represents the rate of the desaturation in the water
198 retention curve, and *m* depends on *n*.

199 In order to perform this study, the parameters defining the water retention curve and
200 hydraulic conductivity functions of the *Reference MOL* and the slope of the interface were set
201 to vary over a range of values that kept the transformed material within the approximate
202 geotechnical category of the *Reference MOL*. The parameters describing the water retention
203 curve and hydraulic conductivity functions of the gas distribution layer remained constant for

all simulations. Table 1 presents the parameters considered in the numerical simulations. The corresponding water retention curves and hydraulic conductivity functions are shown in Figure 1 and Figure 2, respectively.

Table 1: Hydraulic properties of the materials used in the numerical simulations

Figure 1: Water retention curves of the materials used in the parametric analysis

Figure 2: Hydraulic conductivity functions of the materials used in the parametric analysis; (a) $k_{sat\text{-}MOL} = 9\times10^{-6}$ m/s, and (b) $k_{sat\text{-}MOL} = 9\times10^{-4}$ m/s

2.3. Gas flow properties of the methane oxidation layer material

Performing a series of air permeability tests, using a soap flow meter (Bubble-O-Meter; 1-10-500 ml) connected to the inlet of a triaxial cell, the gas intrinsic permeability (K) of the sand-compost mixture used to build the methane oxidation layer of PMOB2 was measured at several initial water content and dry density values (ρ_d). Figure 3 shows the test results as K value at each volumetric air content (θ_a). In order to incorporate the gas flow behavior of the MOL material in the results of numerical simulations, the Ball et al. model (1988) was adopted as the fitting curve for K-θ_a plot, which was consistent with the experimental data (Figure 3).

224

225 Figure 3: Gas intrinsic permeability function of the MOL material for numerical simulations
226 with $k_{sat\text{-}MOL} = 9\times10^{-6}$ m/s

227

228 As shown in Figure 3, the curve can be subdivided into three regions whose frontiers are $\theta_a \approx$
229 5% and $\theta_a \approx 16\%$, herein defined as occlusion value ($\theta_{a\text{-}occ}$) and pre-occlusion value ($\theta_{a\text{-}pocc}$),
230 respectively. The value of *K* is equal to 3.1×10^{-12} (m^2) at $\theta_{a\text{-}pocc}$ and 1.9×10^{-13} (m^2) at $\theta_{a\text{-}occ}$. If
231 the dry density increases, the water content must be decreased in order to maintain θ_a
232 constant. Regardless, the value of *K* is not very affected by the dry density if the volumetric
233 air content, θ_a, remains constant. The values of $\theta_{a\text{-}pocc}$, $\theta_{a\text{-}occ}$ and corresponding *K* values
234 derived from data presented in Figure 3, can be used for any given pair of initial dry density
235 and water content values in the *Reference MOL*.

236 For design purposes, it is hypothesized that biogas flow would be considered reasonably
237 unrestricted when volumetric air content, θ_a, is greater than the pre-occlusion value, $\theta_{a\text{-}pocc}$.
238 Therefore, a practical definition of the *length of unrestricted gas migration*, LUGM, for this
239 sloped PMOB, would be the length, taken horizontally, from the top of the slope to the point
240 where θ_a becomes equal to $\theta_{a\text{-}pocc}$. Beyond this point, gas flow becomes partially restricted
241 and, when it reaches a value of $\theta_a \approx \theta_{a\text{-}occ}$, it is considered blocked. It is reasonable to
242 consider that biogas would prefer to migrate laterally - and find easier escape points – rather
243 than try to flow through a partially restricted area (where $\theta_a \approx \theta_{a\text{-}pocc}$). Changes in dry density
244 (and therefore in porosity) due to settlement or swelling were not considered in the present
245 study.

During numerical simulations, the parameter that was actually monitored was the volumetric water content, θ_w, not the volumetric air content, θ_a. Knowing the initial dry density and porosity of the MOL material, one can calculate $\theta_{w\text{-}pocc}$ (θ_w associated with $\theta_{a\text{-}pocc}$) and $\theta_{w\text{-}occ}$ (θ_w associated with $\theta_{a\text{-}occ}$). The θ_w values obtained from the numerical simulations were then compared with $\theta_{w\text{-}pocc}$ and $\theta_{w\text{-}occ}$.

For simulations No. 1 and No. 7 (Table 1), whose porosities are equal to 0.665, θ_w associated with $\theta_{a\text{-}pocc}$ ($\theta_{w\text{-}pocc}$) is equal to 50.5% and θ_w associated with $\theta_{a\text{-}occ}$ ($\theta_{w\text{-}occ}$) is equal to 61.5%. The van Genuchten parameters that define the water retention curve of the MOL material in simulations No. 3 and No. 9, a = 4.2 and n = 1.28, are associated with the *Reference MOL* compacted to ρ_d = 0.930 kg/m^3 (the porosity was equal to 0.584) (AhouGhalandari et al. 2015). Although the value of $k_{sat\text{-}MOL}$ may change due to compaction, for the case with ρ_d = 0.930 kg/m^3, it remained within the same magnitude as that of the *Reference MOL* (data not presented). Therefore, it seems reasonable to use $\theta_{a\text{-}pocc}$ and $\theta_{a\text{-}occ}$ shown in Figure 3 for simulations No. 3 and No. 9, where $k_{sat\text{-}MOL} = 9\times10^{-6}$ m/s, a = 4.2 and n = 1.28. For these simulations, $\theta_{w\text{-}pocc}$ and $\theta_{w\text{-}occ}$ are equal to 42.4% and 53.4%, respectively. Since the porosities associated with all other simulations in Table 1 are unknown, $\theta_{w\text{-}occ}$ and $\theta_{w\text{-}pocc}$ cannot be calculated for these simulations and, therefore, LUGM cannot be determined. For these cases, only the influence of variables a, n and $k_{sat\text{-}MOL}$ on the distribution of θ_w along the GDL-MOL interface was evaluated.

2.4. Numerical simulations

As previously mentioned, for the purpose of this study, the finite element software SEEP/W (Geo-Slope 2010) was adopted. SEEP/W can mathematically simulate the real physical process of water flowing through a particulate medium.

The simulation using the *Reference MOL* is herein denominated *Reference simulation* (simulation No. 1 in Table 1). For all simulations, the thickness of the methane oxidation layer is 80 cm and the thickness of the gas distribution layer is 40 cm. Figure 4 shows the dimensions, meshing and boundary conditions adopted for the simulations. In order to avoid boundary effects, the length of PMOB in all simulations was considered equal to 100 m. The finite element mesh contained 10,000 elements. The mesh density was higher near the GDL-MOL interface.

Two types of boundary conditions were considered for the simulations: 1) *unit flux function* to assign the seepage reaching the top of the methane oxidation layer, and 2) *zero total flux* boundary condition with *potential seepage face review* at the toe of the simulations in both layers (Figure 4) to represent the drainage system. Water can seep freely across the GDL-MOL interface. Once it has entered the gas distribution layer, it may seep laterally to the toe of the system or move downwards, but it has to be drained out and is no longer of interest, as far as biogas movement across the GDL-MOL is concerned. In the simulations presented herein, the bottom of the model (no flux boundary) coincided with the bottom of the gas distribution layer and water was drained out of the model by means of the two seepage face boundaries shown in Figure 4.

The transient state analysis lasted 246 days. The initial volumetric water content, θ_w, at points located 1 cm above the GDL-MOL interface (herein denominated "*interface points*") were set equal to 35% for all simulations. Water balance components based on climatic data of September 2006 to August 2007 in Quebec (Cabral et al. 2010a) show that the average annual amount of water that seeps into the landfill is equal to 22% of precipitation. Since SEEP/W does not include a soil-atmosphere interaction module (evapotranspiration), the daily seepage rate into the PMOB is therefore considered as 22% of the daily rate of precipitation from March to November 2009 (Figure 5).

Figure 4: Dimensions and boundary conditions of the SEEP/W simulations (slope is variable)

Figure 5: The daily rate of seepage into the PMOB2 during 246 days

3. Results

Data presented in all the figures were obtained from *interface points*. The nodes located in the first and last 5 meters of the modelled passive methane oxidation biosystems (PMOBs) were not considered in the analyses, in order to avoid potential boundary effects.

3.1. Reference simulation

Figure 6 shows volumetric water content (θ_w) values of the *interface points* at several time steps during the *Reference simulation*, which lasted 246 days. The initial θ_w = 35.0% is associated with a degree of saturation equal to 53% and gravimetric water content equal to 47%, which means compaction on the dry side of the line of optima, i.e. at water contents lower than those given by the optimum water contents of each individual compaction curve.

θ_w increased towards the bottom of the slope, but the difference in θ_w values from the top to bottom were quite small. The difference between maximum and minimum values of θ_w along the interface, referred to as $\Delta\theta_w$, increased with time. This parameter gives an idea of the level of uniformity of θ_w along the interface; the higher it is, the greater the chance of a non-uniform interface, as far as moisture distribution is concerned. The opposite is rather

straightforward: the lower $\Delta\theta_w$ is, the greater the chance of uniformity in distribution of moisture.

During the simulation period, the maximum $\Delta\theta_w$ (1.5%) occurred on Day 208, when θ_w of the *interface points* had already reached the volumetric water content associated with pre-occlusion value, $\theta_{w\text{-}pocc}$. In other words, upward gas migration was already partially restricted. Prior to the onset of $\theta_{w\text{-}pocc}$, which was equal to 50.5% and occurred on Day 141, the maximum value of $\Delta\theta_w$ was equal to 8.8×10^{-3} %. This very small value leads to the conclusion that the interface had become uniform, as far as volumetric water content was concerned. Therefore, once the $\theta_{w\text{-}pocc}$ was attained, the length of unrestricted gas migration, LUGM, abruptly became equal to zero.

During the last 105 days of the *Reference simulation,* $\theta_w > \theta_{w\text{-}pocc}$, meaning that upward biogas flow was restricted along the interface. Biogas would therefore migrate within the gas distribution layer towards the top of the slope or escape through preferential pathways, such as cracks on the final cover. The CH_4 in the biogas transported through these preferential flow paths would less likely be submitted to biotic oxidation (Chanton et al. 2011).

The maximum value of θ_w ($\theta_{w\text{-}max}$) was equal to 53.3%, which was lower than $\theta_{w\text{-}occ}$ (61.5%) but greater than $\theta_{w\text{-}pocc}$ (50.5%). Therefore, despite the fact that the pores at the interface of the *Reference simulation* never became completely occluded ($\theta_w > \theta_{w\text{-}occ}$), it is recommended to use a conservative approach and consider gas migration to be restricted when $\theta_w > \theta_{w\text{-}pocc}$.

Before attainment of $\theta_{w\text{-}max}$, the value of θ_w at the *interface points* increased continuously, independent of the transient seepage rate. After that, θ_w fluctuated depending on the seepage rate.

Figure 6: Distribution of θ_w in *interface points* at several time steps in simulation No. 1 (*Reference simulation*)

Figure 7 presents the K values of the *interface points*, at several time steps during the *Reference simulation*. K decreased continuously with time and, on Day 141, all K values of the *interface points* fell below the pre-occlusion value, i.e. $K = 2.1\times10^{-12}$ m^2. The lowest value of K during the simulation period was 1.4×10^{-12} m^2.

Before pre-occlusion, the maximum value of K_{max}/K_{min} occurred on Day 129 and was equal to 1.0007. In other words, there was very little variability in K along the interface up to this time. This is expected, given the small variation in moisture content along the interface. During the analysis, the maximum value of K_{max}/K_{min} was equal to 1.25, and occurred on Day 208.

Figure 7: Distribution of K in *interface points* at several time steps, for simulation No. 1

3.2. Effect of the pore size distribution

The parameter n in the Van Genuchten (1980) equation represents the rate of desaturation of the soil. The greater the value of n, the steeper the slope of the water retention curve, and the easier to drain (desaturate) the soil (Fredlund et al. 2002). Since the shape of the grain size distribution curve is similar to the shape of the water retention curve, the former is often used to estimate the latter (e.g. Arya and Paris 1981; Fredlund et al. 2002). In practical terms, the

360 steeper the grain size distribution curve, the steeper the slope of the desaturation zone of the
361 water retention curve.

362

363 Figure 8: Distribution of θ_w in *interface points* at several time steps, for simulation No. 2

364

365 For simulation No. 2, the value of the van Genuchten parameter *n* of the *Reference MOL* was
366 increased to 1.5, while the values of *a*, $k_{sat\text{-}MOL}$ and initial θ_w remained constant. The variation
367 of θ_w with distance is presented in Figure 8. In this case, in order to evaluate whether or not
368 there was pre-occlusion, a value of $\theta_{w\text{-}pocc}$ had to be adopted, since it was not obtained in the
369 laboratory for this simulated methane oxidation layer. For simulations No. 2 and No. 8 the
370 same $\theta_{w\text{-}pocc}$ value of the *Reference MOL* was adopted.

371 The results of the simulation showed that the maximum $\Delta\theta_w$ occurred on Day 210 and an
372 increase in *n* led to a reduction in the value of θ_w and therefore, to an unrestricted gas flow
373 across the interface. Indeed, $\theta_{w\text{-}max}$ attained 47.0%, which is lower than $\theta_{w\text{-}pocc}$. However, the
374 validity of these results relies on the presupposition that it was reasonable to adopt the same
375 $\theta_{w\text{-}pocc}$ value as that of the *Reference MOL*. This hypothesis was verified as discussed in the
376 remainder of this section.

377 In Figure 9, the water retention curve of the *Reference MOL* is compared with the water
378 retention curve of two other materials from other studies. As shown in Figure 10 (also see
379 Figure 3 for the *Reference MOL*), the shapes of gas permeability functions of these materials
380 are similar, insofar as the occurrence of pre-occlusion can be clearly identified. In the case of
381 the clay, the volumetric air content at pre-occlusion, $\theta_{a\text{-}pocc}$, was equal to ~12% (Figure 10a),
382 whereas for the silty sand it was ~17% (Figure 10b) ($\theta_{a\text{-}pocc} \approx 16$ % for the *Reference MOL*).

383 According to Figure 9, the steepest slope of the desaturation zone was associated with the
384 clay studied by Jucá and Maciel (2006), followed by the silty sand tested by Springer et al.
385 (1998), and the sand-compost mixture of the *Reference MOL*. Therefore, the clay possessed
386 the greatest value of *n*. The results presented in Figure 9 and Figure 10 showed that materials
387 with different textures and desaturation slopes (as expressed by *n*) may exhibit rather similar
388 values of $\theta_{a\text{-}pocc}$. Based on this limited analysis, it was assumed that changing the value of *n*
389 from 1.28 (adopted for the *Reference MOL*) to 1.5 would not lead to much of a difference in
390 $\theta_{a\text{-}pocc}$.

391

392 Figure 9: The water retention curve of the *Reference MOL* and materials from other studies
393 (Jucá and Maciel 2006; Springer et al. 1998)

394

395 Figure 10: variation of (a) coefficient of air permeability and (b) gas intrinsic permeability
396 with θ_a in materials from other studies (Jucá and Maciel 2006; Springer et al. 1998)

397

398 In Figure 11, two grain size distribution curves were derived from the water retention curves:
399 one for the *Reference MOL* (*a* = 2.8 and *n* =1.28) and the other for the modified *Reference*
400 *MOL* (*a* = 2.8 and *n* = 1.5). In order to obtain the material with *n* = 1.5, the amount of
401 compost whose particles have a diameter less than 0.4 mm had to be artificially decreased
402 and substituted by a granular soil, such as sand. It is as if there was more sand in the mixture.
403 Such substitution entails a slight change in specific gravity and saturated volumetric water
404 content (θ_s, which is equal to porosity). Since the initial dry density, $\theta_{a\text{-}pocc}$ and the porosity of
405 the material remained similar, $\theta_{w\text{-}pocc}$ remained almost unaltered. Consequently, increasing *n*

406 to 1.5 resulted in only a slight change in $\theta_{w\text{-}pocc}$, the control parameter based on which the
407 results of the simulations were analyzed.

408

409 Figure 11: Corresponding grain size distribution curves of the water retention curves of the
410 MOL materials for two cases (a=2.8 and n=1.28; a=2.8 and n=1.5), using the Fredlund et al.
411 equation (2002)

412

413 **3.3. Effect of initial dry density**

414 The effect of compaction on the value of gas permeability has been the subject of several
415 studies both in soil mechanics (e.g. Leroueil and Hight 2013; Tang et al. 2011) and dealing
416 with methane oxidation efficiency of passive methane oxidation biosystems (e.g. Gebert et al.
417 2011; Rachor et al. 2011). It can be expected that an increase in dry density results in a
418 higher air entry value, therefore greater values of a, while the slope of the desaturation zone
419 of the water retention curve (n) remains unchanged (Mirzaii and Yasrobi 2012; Nuth and
420 Laloui 2008). The same behavior was observed in the material constituting the *Reference*
421 *MOL* (AhouGhalandari et al. 2015). Therefore, the results obtained from simulations where
422 the value of a was increased from 2.8 to 4.2, are expected to incorporate the effect of a higher
423 initial dry density of the methane oxidation layer on the distribution of θ_w values along the
424 GDL-MOL interface.

425

426 Figure 12: Distribution of θ_w in *interface points* at several time steps, for simulation No. 3

427

Figure 12 shows the results of simulation No. 3, for which the initial θ_w was equal to 35.0%. The initial θ_w corresponds to the degree of saturation equal to 60% and gravimetric water content equal to 38%, indicating that the material was compacted dry of optima. As a result of increasing the initial dry density of the MOL material, θ_w at the *interface points* exceeded both $\theta_{w\text{-}pocc}$ (42.7%) and $\theta_{w\text{-}occ}$ (53.4%) on Days 64 and 132, respectively. It is noteworthy to recall that $\theta_{w\text{-}occ}$ was not attained during the *Reference simulation*. Prior to the onset of pre-occlusion, the maximum $\Delta\theta_w$ was equal to 0.0049%; by all means a nearly negligible difference in moisture content between the top and bottom of the slope. Therefore, the value of LUGM abruptly became equal to zero when $\theta_{w\text{-}pocc}$ was attained. The maximum $\Delta\theta_w$ occurred on Day 207.

3.4. Effect of $k_{sat\text{-}MOL}$

Figure 13 shows θ_w values at the *interface points* for several time steps of simulations No. 4 to No. 6. For these simulations, the $k_{sat\text{-}MOL}$ was 9×10^{-4} m/s, i.e. 100 times greater than the $k_{sat\text{-}MOL}$ of the *Reference MOL*. Since the materials corresponding to simulations No. 4 to No. 6 were not characterized, the values of $\theta_{w\text{-}pocc}$ and $\theta_{w\text{-}occ}$ are unknown. Consequently, it was not possible to clearly evaluate whether or not the *interface points* ever reached pre-occlusion or occlusion.

The results in Figure 13 show that, at each time step, the increase in $k_{sat\text{-}MOL}$ led to greater variations in θ_w along the interface, towards the bottom of the slope. In other words, $\Delta\theta_w$ for these simulations were greater than those obtained with the corresponding simulations with $k_{sat\text{-}MOL} = 9\times10^{-6}$ m/s, i.e. *Reference simulation* and simulations No. 2 and No. 3. The maximum values of $\Delta\theta_w$ during simulations No. 4 to No. 6 occurred on Day 207. The evolution of θ_w with time in simulations No. 4 to No. 6 was consistent with the variation in

seepage rate with time (Figure 5); a clear indication of the sensitivity of the modeled system to the seepage rate, due to the value of $k_{sat\text{-}MOL}$.

Figure 13: Distribution of θ_w in *interface points* at several time steps, for (a) simulation No. 4, (b) simulation No. 5, and (c) simulation No. 6

3.5. Effect of slope

Figure 14, shows the results of simulations No. 7 to No. 9, which used the same materials as simulations No. 1 to No. 3, respectively (Table 1). However, in these cases, the model was built with a steeper slope (10%). Simulation No. 7 (Figure 14a) was quite similar to the *Reference simulation*, insofar as the value of LUGM became equal to zero quite abruptly; and both on Day 141. LUGM abruptly became equal to zero on Day 64 in simulation No. 9 (Figure 14c), and on Day 132 the interface had become completely occluded. The change in slope from 3.5% to 10% led to very slight changes in θ_w along the interface. This is valid when comparing simulations No. 1 and No. 7, No. 2 and No. 8 and No. 3 and No. 9.

Figure 14: Distribution of θ_w in *interface points* at several time steps, for (a) simulation No. 7, (b) simulation No. 8, and (c) simulation No. 9

Figure 15 shows the results of simulations No. 10 to No. 12, whose interfaces were steeper than interfaces in simulations with the same materials (No. 4 to No. 6; see Table 1). As can be observed in Figure 15, at each time step, increasing the slope of the interface resulted in a radically greater variation in θ_w along the interface.

Figure 15: Distribution of θ_w in *interface points* at several time steps, for (a) simulation No. 10, (b) simulation No. 11, and (c) simulation No. 12

4. Discussion

Figure 16 presents the effect of slope, $k_{sat\text{-}MOL}$, the van Genuchten parameters *a* and *n* on maximum value of volumetric water content ($\theta_{w\text{-}max}$) at the *interface points* of all simulations. It can be observed that the values of $\theta_{w\text{-}max}$ decreased very slightly with the increase in slope of the interface. Regardless of the value of the slope and $k_{sat\text{-}MOL}$, increasing the van Genuchten parameter *a* (which can be attributed to greater compaction) resulted in a large increase in $\theta_{w\text{-}max}$, i.e. the air-filled pores at *interface points* were more likely to be occluded (more precisely, to reach $\theta_{w\text{-}pocc}$ or $\theta_{w\text{-}occ}$).

For each value of *a*, *n* and slope, increasing the $k_{sat\text{-}MOL}$ very slightly increased the value of $\theta_{w\text{-}max}$. However, important drops in the values of θ_w and $\theta_{w\text{-}max}$ at *interface points* were observed following an increase in the value of *n*. For example, increasing *n* of the *Reference MOL* (Simulation No. 2; Figure 8) led to a value of LUGM equal to the total length of the interface, i.e. it remained completely unrestricted throughout the duration of the simulation, whereas in the actual *Reference simulation*, LUGM became equal to 0 (total occlusion) half-way through the simulation (Day 141).

Figure 16: $\theta_{w\text{-}max}$ values in *interface points*, for several values of *a*, *n*, $k_{sat\text{-}MOL}$ and slope

497 It stems from these analyses that among the variables evaluated in the present study, *n* is the
498 one that most influenced $\theta_{w\text{-}max}$, therefore the response of the PMOB to upward gas
499 migration. In simpler terms, *n* is a fundamental parameter in PMOB design, since it is
500 determinant in reducing the risk of attaining pore occlusion, which restricts upward gas
501 migration across the GDL-MOL interface. When partial occlusion occurs, biogas flows
502 laterally within the gas distribution layer towards the top of the slope, where it can escape to
503 the atmosphere. Of course, biogas can also escape through preferential pathways, such as
504 cracks within the final cover (tension cracks are common near the top of slopes) or voids
505 around protruding instrumentations and collection wells. In all these cases, hotspots, a
506 recurring problem in landfills, are created.

507 In Figure 17, the maximum values of $\Delta\theta_w$ are plotted as a function of slope, $k_{sat\text{-}MOL}$, *a* and *n*.
508 For simulations with $k_{sat\text{-}MOL} = 9.4\times10^{-6}$ m/s, increasing *a* and slope had a minor effect on the
509 maximum $\Delta\theta_w$. However, increasing *n* led to large variations of θ_w (greater $\Delta\theta_w$). For certain
510 types of designs, such as the jagged interface proposed by Kjeldsen et al. (2013), it is
511 important to maintain θ_w at the top of each segment sufficiently lower than at the bottom to
512 increase the chances that a sufficiently large "channel" allows upward migration of CH_4 to be
513 oxidized within the methane oxidation layer.

514 In the cases where $k_{sat\text{-}MOL}$ was 100 times greater (9.4×10^{-4} m/s), increasing *a*, *n* and slope,
515 considerably increased the maximum $\Delta\theta_w$. Accordingly, depending on the value of $k_{sat\text{-}MOL}$,
516 the other 3 variables (*a*, *n* and slope) may have an important role in controlling the pattern of
517 upward flow of biogas, and reducing the chances of localized emissions (hotspots).

518

519 Figure 17: Maximum $\Delta\theta_w$ in *interface points*, for several values of *a*, *n*, $k_{sat\text{-}MOL}$ and slope

520

Figure 18 shows the day when the maximum value of the volumetric water content $\theta_{w\text{-}max}$ was attained for several simulations. As presented in the previous section, the time associated with the onset of maximum $\Delta\theta_w$ was quite similar for all simulations, i.e. Days 207-212. According to Figure 18, for simulations with *n* or slope greater than those of the *Reference simulation*, $\theta_{w\text{-}max}$ was attained earlier than maximum $\Delta\theta_w$. In other words, from the moment when $\theta_{w\text{-}max}$ was attained until the onset of maximum $\Delta\theta_w$ the *interface points* were continuously drained, particularly towards the top of the slope. The temporary drainage of *interface points* may be considered as an advantageous effect, as far as unrestricted upward flow of biogas is concerned. For the simulations with *n* or slope equal to those of the *Reference simulation*, $\theta_{w\text{-}max}$ was attained later than maximum $\Delta\theta_w$ (gray area in Figure 18). Therefore, between the onset of $\theta_{w\text{-}max}$ and the moment when the maximum $\Delta\theta_w$ was attained, the interface became wetter.

Figure 18: The time associated with attaining the $\theta_{w\text{-}max}$ in *interface points*, for several values of *a*, *n*, $k_{sat\text{-}MOL}$ and slope

5. Conclusions

This study and the simulations thereof aimed at evaluating how variations in the main hydraulic parameters affected the behavior of a modelled passive methane oxidation biosystem (PMOB), as far as biogas migration and loading distribution at the base of the methane oxidation layer is concerned. Ideally, all of the candidate MOL materials should be characterized to obtain their hydraulic parameters and gas flow properties. Indeed, the volumetric water content values at pre-occlusion and/or occlusion ($\theta_{w\text{-}pocc}$ and/or $\theta_{w\text{-}occ}$),

544 which correspond to the volumetric air content values at pre-occlusion and/or occlusion (θ_{a-pocc} and/or θ_{a-occ}), should be known before performing numerical simulations. Analysis of the
546 performance would therefore be straightforward: the distance from the top to the point where
547 θ_{w-pocc} occurred (i.e. the length of unrestricted gas migration, LUGM) would be determined
548 from the simulations. Designs would be based on an optimization of the value of LUGM, and
549 not necessarily on its maximum possible value, i.e. the entire length of the interface. Good
550 practice calls for a compromise between CH_4 oxidation efficiency and the cost of materials to
551 construct the PMOB. Unfortunately, it was beyond the scope of this study to determine the
552 hydraulic and gas flow parameters of all the materials considered in the simulations presented
553 herein. The value of this study relies on the identification of the relative importance of the
554 main variables involved.

555 Increasing either the van Genuchten parameter associated with the slope of the desaturation
556 zone in the water retention curve (n), the saturated hydraulic conductivity of MOL material
557 ($k_{sat-MOL}$) or the slope, resulted in greater differences in volumetric water content along the
558 interface. For plane interfaces (such as the one presented in this study), greater differences in
559 volumetric water content may result in a LUGM that is shorter than the total length of the
560 interface. As far as the van Genuchten parameter a is concerned, the greater its value, the
561 greater are the chances that moisture in the pores at the *interface points* will increase enough
562 to restrict upward gas flow.

563 The maximum suction values in all simulations were sufficiently high to prevent seepage of
564 water from the methane oxidation layer into the gas distribution layer for a capillary barrier
565 with the methane oxidation layer acting as a moisture retaining layer and the gas distribution
566 layer as a capillary block layer (data not presented). However, these suction levels were low
567 enough to allow the air-filled pores of the methane oxidation layer to be in a state of
568 occlusion or pre-occlusion, and therefore to divert upward migrating biogas upslope. One

limitation of the numerical simulations presented relates to the fact that water generation due to microbial activity was not considered. This might lead to lower suction values (higher moisture) near the GDL-MOL interface, therefore changing the pattern of biogas migration. However, in order to integrate this properly into numerical simulations, the effects of increased temperature on evaporation and plant transpiration would also have to be considered in the transient state simulations.

Acknowledgements

This study received financial support from the Natural Science and Engineering Research Council of Canada (NSERC) and Waste Management (WM Quebec Inc.), under the collaborative research and development grant # CRD 379885-08, from the Consortium de recherche et innovations en bioprocédés industriels du Québec (CRIBIQ) and from Discovery Grant #170226. The Authors would like to acknowledge the invaluable help of Jean-Guy Lemelin, technician, and of Philippe Tétrault, formerly with the Geoenvironmental Group at the Université de Sherbrooke.

References

Adu-Wusu, C., and Yanful, E.K. 2006. Performance of Engineered Test Covers on Acid-Generating Waste Rock at Whistle Mine, Ontario. Canadian Geotechnical Journal **43**(1): 1-18.

AhouGhalandari, B., Cabral, A.R., and Leroueil, S. 2015. Assessment of Biogas Distribution at the Base of Passive Methane Oxidation Biosystems. *In* The XV Panamerican Conference on Soil Mechanics and Geotechnical Engineering, Buenos Aires, Argentina.

591 Arya, L.M., and Paris, J.F. 1981. A Physicoempirical Model to Predict the Soil Moisture
592 Characteristic from Particle-Size Distribution and Bulk Density Data. Soil Science Society of
593 America Journal **45**: 1023-1030
594 ASTM-D2434-68. 2006. Standard Test Method for Permeability of Granular Soils (Constant
595 Head). ASTM International, West Conshohocken, PA.
596 Aubertin, M., Cifuentes, E., Martin, V., Apithy, S., Bussiere, B., Molson, J., Chapuis, R.P., and
597 Maqsoud, A. 2006. An Investigation of Factors that Influence the Water Diversion Capacity of
598 Inclined Covers with Capillary Barrier Effects. Geotechnical Special Publication, American
599 Society of Civil Engineers **147**: 613-624.
600 Ball, B.C., O'Sullivan, M.F., and Hunter, R. 1988. Gas Diffusion, Fluid Flow and Derived Pore
601 Continuity Indices in Relation to Vehicle Traffic and Tillage. Journal of Soil Science **39**: 327-
602 339.
603 Bohn, S., and Jager, J. 2009. Microbial Methane Oxidation in Landfill top Covers - Process
604 Study on an MBT Landfill. *In* 12th International Waste Management and Landfill Symposium.
605 CISA, Margherita di Pula, Italy.
606 Bussière, B., Apithy, S., Aubertin, M., and Chapuis, R.P. 2003a. Diversion Capacity of Sloping
607 Covers with Capillary Barrier Effect. *In* The 56th Annual Canadian Geotechnical Conference,
608 4th Joint IAH-CNC, and CGS Groundwater Specialty Conference & 2003 NAGS Conference,
609 Winnipeg, Manitoba, Canada.
610 Bussière, B., Aubertin, M., and Chapuis, R.P. 2003b. The Behavior of Inclined Covers Used
611 as Oxygen Barriers. Canadian Geotechnical Journal **40**: 512-535.
612 Cabral, A.R., Létourneau, M., Yanful, E., Song, Q., McCartney, J.S., and Parks, J. 2010a.
613 Geotechnical Issues in the Design and Construction of PMOBs. *In* UNSAT 2010, Barcelona.
614 pp. 1361-1367.

615 Cabral, A.R., Moreina, J.F.V., and Jungia, L.B. 2010b. Biocover Performance of Landfill
616 Methane Oxidation: Experimental Results. Journal of Environmental Engineering **136**: 785-
617 793.
618 Capanema, M.A., and Cabral, A.R. 2012. Evaluating Methane Oxidation Efficiencies in
619 Experimental Landfill Biocovers by Mass Balance and Carbon Stable Isotopes. Water Air Soil
620 Pollut **223**(9): 5623-5635.
621 Chanton, J., Abichou, T., Langford, C., Hater, G., Green, R., Goldsmith, D., and Swan, N.
622 2011. Landfill Methane Oxidation Across Climate Types in the U.S. Environ. Sci. Technol.
623 **45**: 313-319.
624 Chapuis, R.P. 2004. Predicting the Saturated Hydraulic Conductivity of Sand and Gravel Using
625 Effective Diameter and Void Ratio. Can. Geotech. J. **41**: 787-795.
626 Dagenais, A.-M., Aubertin, M., Bussiere, B., and Cyr, J. 2005. Performance of the Lorraine
627 Mine Site Cover to Limit Oxygen Migration *In* 2005 SME Annual Meeting: Got Mining
628 Annual Meeting: Got Mining - Preprints, Society for Mining, Metallurgy and Exploration,
629 Littleton, CO 80127-4102, United States,, Salt Lake City, UT, United States pp. 843-857
630 Fredenslund, A.M., Scheutz, C., and Kjeldsen, P. 2010. Tracer Method to Measure Landfill
631 Gas Emissions from Leachate Collection Systems. Waste Management **30**: 2146–2152.
632 Fredlund, M.D., Wilson, G.W., and Fredlund, D.G. 2002. Use of the Grain-Size Distribution
633 for Estimation of the Soil-Water Characteristic Curve. Canadian Geotechnical Journal **39**:
634 1103-1117.
635 Gebert, J., Groengroeft, A., and Pfeiffer, E.M. 2011. Relevance of Soil Physical Properties for
636 the Microbial Oxidation of Methane in Landfill Covers. Soil Biol Biochem **43**: 1759-1767.
637 Geck, C., Gebert, J., Scharff, H., Streese-Kleeberg, J., and Pfeiffer, E.-M. 2012. Heterogeneous
638 Gas Distribution within a Biocover Designed for Methane Oxidation *In* 7th Intercontinental
639 Landfill Research Symposium (ICLRS). Poster presentation, Luleä, Sweden.

640 GEO-SLOPE. 2010. Seepage Modeling with SEEP/W 2007. *Edited by* G.-S.I. Ltd.
641 Huber-Humer, M., Röder, S., and Lechner, P. 2009. Approaches to Assess Biocover
642 Performance on Landfills. Waste Management **29**: 2092-2104.
643 HYPROP-UMS. 2013. HYPROP-UMS User's Manual. *In* Art. no. HYPROP Version 02. UMS
644 GmbH München.
645 Jucá, J., and Maciel, F. 2006. Gas Permeability of a Compacted Soil Used in a Landfill Cover
646 Layer. *In* Fourth International Conference on Unsaturated Soils. *Edited by* G.A. Miller and
647 C.E. Zapata and S.L. Houston and D.G. Fredlund. American Society of Civil Engineers,
648 Carefree, Arizona, United States. pp. 1535-1546.
649 Khire, M.V., Benson, C.H., and Bosscher, P.J. 2000. Capillary barriers: Design variables and
650 water balance. Journal of Geotechnical and Geoenvironmental Engineering **126**(8): 695-708.
651 Kjeldsen, P., Skov, B., Cassini, F., Zishen, M., and Scheutz, C. 2013. Mitigation of Methane
652 Emissions in a Pilot-Scale Biocover System at the Av Milo Landfill, Denmark: System Design
653 and Gas Distribution. *In* 14th International Waste Management and Landfill Symposium CISA
654 Publisher S. Margherita di Pula, Cagliari, Italy
655 Langfelder, L.J., Chen, C.F., and Justice, J.A. 1968. Air Permeability of Compacted Cohesive
656 Soils. Journal of the Soil Mechanics and Foundations Division **94**(4): 981-1002.
657 Leroueil, S., and Hight, D.W. 2013. Compacted Soils: From Physics to Hydraulic and
658 Mechanical Behaviour. *In* First Pan-American Conference on Unsaturated Soils. *Edited by*
659 C.M. Bernardo Caicedo, Laureano Hoyos, Julio Esteban Colmenares, Ivan Rafael Berdugo,
660 Cartagena, Colombia. pp. 41-59.
661 Maciel, F., and Jucá, J. 2000. Laboratory and Field Tests for Studying Gas Flow Through MSW
662 Landfill Cover. *In* Geo-Denver. *Edited by* C.D. Shackelford and S.L. Houston and N.Y. Chang.
663 American Society of Civil Engineers, Denver, Colorado, United States. pp. 569-585.

664 Marinho, F.A.M., Andrade, M.C.J., and Jucá, J.F.T. 2001. Air and Water Permeability of a
665 Compacted Soil Used in a Solid Waste Landfill in Recife, Brazil. *In* the Third BGA
666 Geoenvironmental Engineering Conference. Thomas Telford Publishing, Thomas Telford Ltd.,
667 Edinburg, Scotland. pp. 437-442.
668 Mirzaii, A., and Yasrobi, S.S. 2012. Influence of Initial Dry Density on Soil-Water
669 Characteristics of Two Compacted Soils. Géotechnique Letters **2**: 193-198.
670 Mualem, Y. 1976. A new model for predicting the hydraulic conductivity of unsaturated porous
671 media. Water Resources Research **12**: 513-522.
672 Ndanga, É.M., Bradley, R.L., and Cabral, A.R. 2015. Does Vegetation Affect the Methane
673 Oxidation Efficiency of Passive Biosystems? Waste Management **38**: 240-249.
674 Nuth, M., and Laloui, L. 2008. Advances in Modelling Hysteretic Water Retention Curve in
675 Deformable Soils. Computers and Geotechnics **35**: 835-844.
676 Pokhrel, D., Hettiaratchi, P., and Kumar, S. 2011. Methane Diffusion Coefficient in Compost
677 and Soil-Compost mixtures in Gas Phase Biofilter. Chem Eng J **169**: 200-206.
678 Rachor, I., Gebert, J., Gröngröft, A., and Pfeiffer, E.M. 2011. Assessment of the Methane
679 Oxidation Capacity of Compacted Soils Intended for Use as Landfill Cover Materials. Waste
680 Management **31**: 833-842.
681 Roncato, C.D.L., and Cabral, A.R. 2012. Evaluation of Methane Oxidation Efficiency of Two
682 Biocovers: Field and Laboratory Results. Journal of Environmental Engineering **138**(2): 164-
683 173.
684 Röwer, I.U., Gebert, J., Streese-Kleeberg, J., Kleinschmidt, V., Melchior, S., Scharff, H., and
685 Pfeiffer, E.-M. 2012. Heterogeneous Emission from a Biocover Designed for Methane
686 Oxidation. *In* 7th Intercontinental Landfill Research Symposium (ICLRS). Poster presentation,
687 Luleä, Sweden.

688 Sadasivam, B.Y., and Reddy, K.R. 2014. Landfill Methane Oxidation in Soil and Bio-Based
689 Cover Systems: a Review. Rev Environ Sci Biotechnol **13**: 79-107.
690 Scheutz, C., Fredenslund, A.M., Chanton, J., Pedersen, G.B., and Kjeldsen, P. 2011. Mitigation
691 of Methane Emission from Fakse Landfill Using a Biowindow System. Waste Management
692 **31**: 1018-1028.
693 Springer, D.S., Loaiciga, H.A., Cullen, S.J., and Everett, L.G. 1998. Air Permeability of Porous
694 Materials Under Controlled Laboratory Conditions. Groundwater **36**(4): 558-565. doi:
695 10.1111/j.1745-6584.1998.tb02829.x.
696 Stormont, J.C. 1996. The Effectiveness of Two Capillary Barriers on a 10% Slope.
697 Geotechnical and Geological Engineering Journal **14**: 243-267.
698 Tang, A.M., Cui, Y.-J., Richard, G., and Défossez, P. 2011. A Study on the Air Permeability
699 as Affected by Compression of Three French Soils. Geoderma **162**: 171-181.
700 Tétreault, P., Cabral, A.R., and Abdolahzadeh, A.M. 2013. Non-Uniform Distribution of
701 Biogas under a Biocover due to Capillary Barrier Effect: Case Studies. *In* GEOMontreal,
702 Montreal, Canada.
703 Vachon, B.L., Abdolahzadeh, A.M., and Cabral, A.R. 2015. Predicting the Diversion Length
704 of Capillary Barriers Using Steady State and Transient State Numerical Modeling: Case Study
705 of the Saint-Tite-des-Caps Landfill Final Cover. Can. Geotech. J. **52**: 2141-2148.
706 van Genuchten, M.T. 1980. A closed-form equation for predicting the hydraulic conductivity
707 of unsaturated soils. Soil Science Society of America Journal **44**: 892-898.
708 Williams, D.J., Wilson, G.W., and Currey, N.A. 1997. A cover system for a potentially acid
709 forming waste rock dump in a dry climate. *In* 4th International Conference on Tailings and
710 Mine Waste 97. Balkema, Rotterdam, Fort Collins, CO. pp. 231–235.

711 Wilson, G.W., Barbour, S.L., Swanson, D., and O'Kane, M. 1995. Instrumentation and
712 Modelling for Saturated/Unsaturated Performance of Soil Covers for Acid Generating Waste
713 Rock Hydrogéologie **4**: 99-108.
714 Yanful, E.K. 1993. Oxygen Diffusion through Soil Covers on Sulphidic Mine Tailings. Journal
715 of Geotechnical Engineering **119**(8): 1207-1228.

List of tables

List of figures

Figure 15: Distribution of θ_w in *interface points* at several time steps, for (a) simulation No. 10, (b) simulation No. 11, and (c) simulation No. 12

Figure 16: $\theta_{w\text{-}max}$ values in *interface points*, for several values of *a*, *n*, $k_{sat\text{-}MOL}$ and slope

Figure 17: Maximum $\Delta\theta_w$ in *interface points*, for several values of *a*, *n*, $k_{sat\text{-}MOL}$ and slope

Figure 18: The time associated with attaining the $\theta_{w\text{-}max}$ in *interface points*, for several values of *a*, *n*, $k_{sat\text{-}MOL}$ and slope

Table 1: Hydraulic properties of the materials used in the numerical simulations

Simulation No.	Slope	MOL (sand-compost)					GDL (gravel)				
		a (kPa)	n	k_{sat} (m/s)	θ_s (%m^3/m^3)	θ_r (%m^3/m^3)	a (kPa)	n	k_{sat} (m/s)	θ_s (%m^3/m^3)	θ_r (%m^3/m^3)
(1)	3.5%	2.8	1.28								
(2)	3.5%	2.8	1.5	1.9×10^{-6}							
(3)	3.5%	4.2	1.28								
(4)	3.5%	2.8	1.28								
(5)	3.5%	2.8	1.5	1.9×10^{-4}							
(6)	3.5%	4.2	1.28		67.0	0.17	0.5	2.4	4.3×10^{-2}	30.0	0.0
(7)	10%	2.8	1.28								
(8)	10%	2.8	1.5	1.9×10^{-6}							
(9)	10%	4.2	1.28								
(10)	10%	2.8	1.28								
(11)	10%	2.8	1.5	1.9×10^{-4}							
(12)	10%	4.2	1.28								

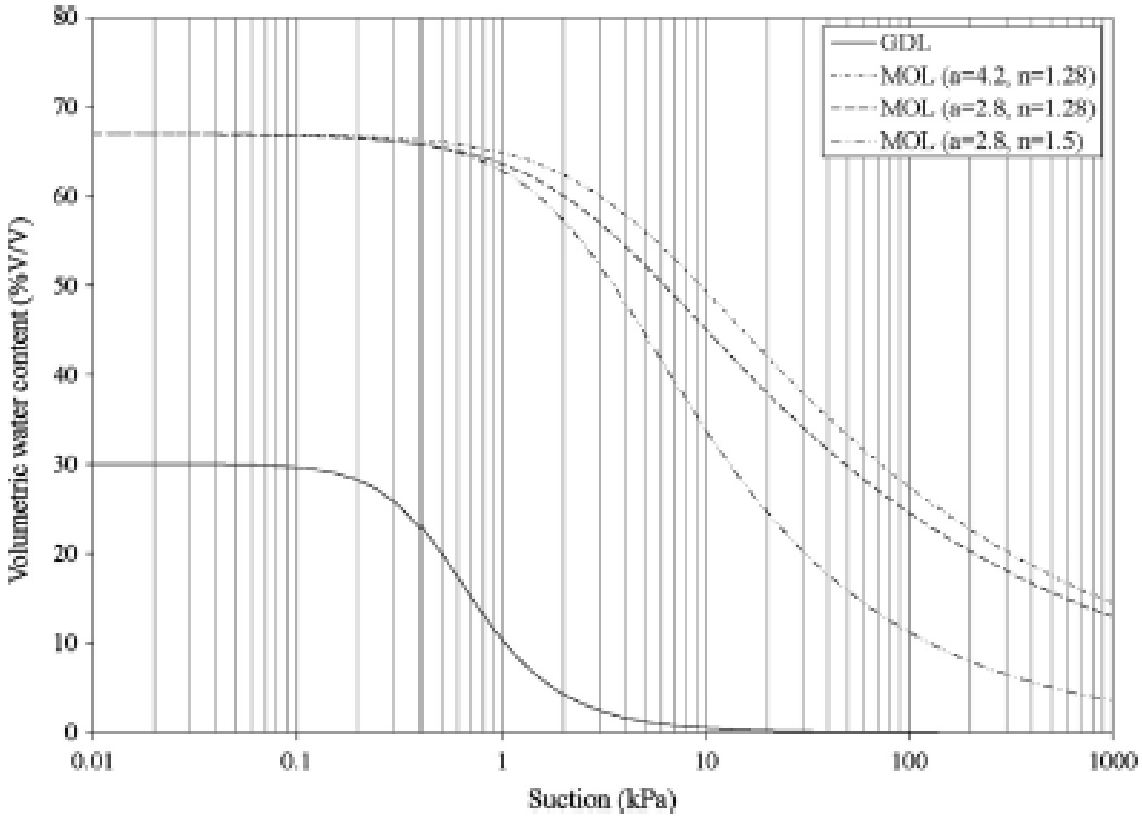

Figure 1: Water retention curves of the materials used in the parametric analysis

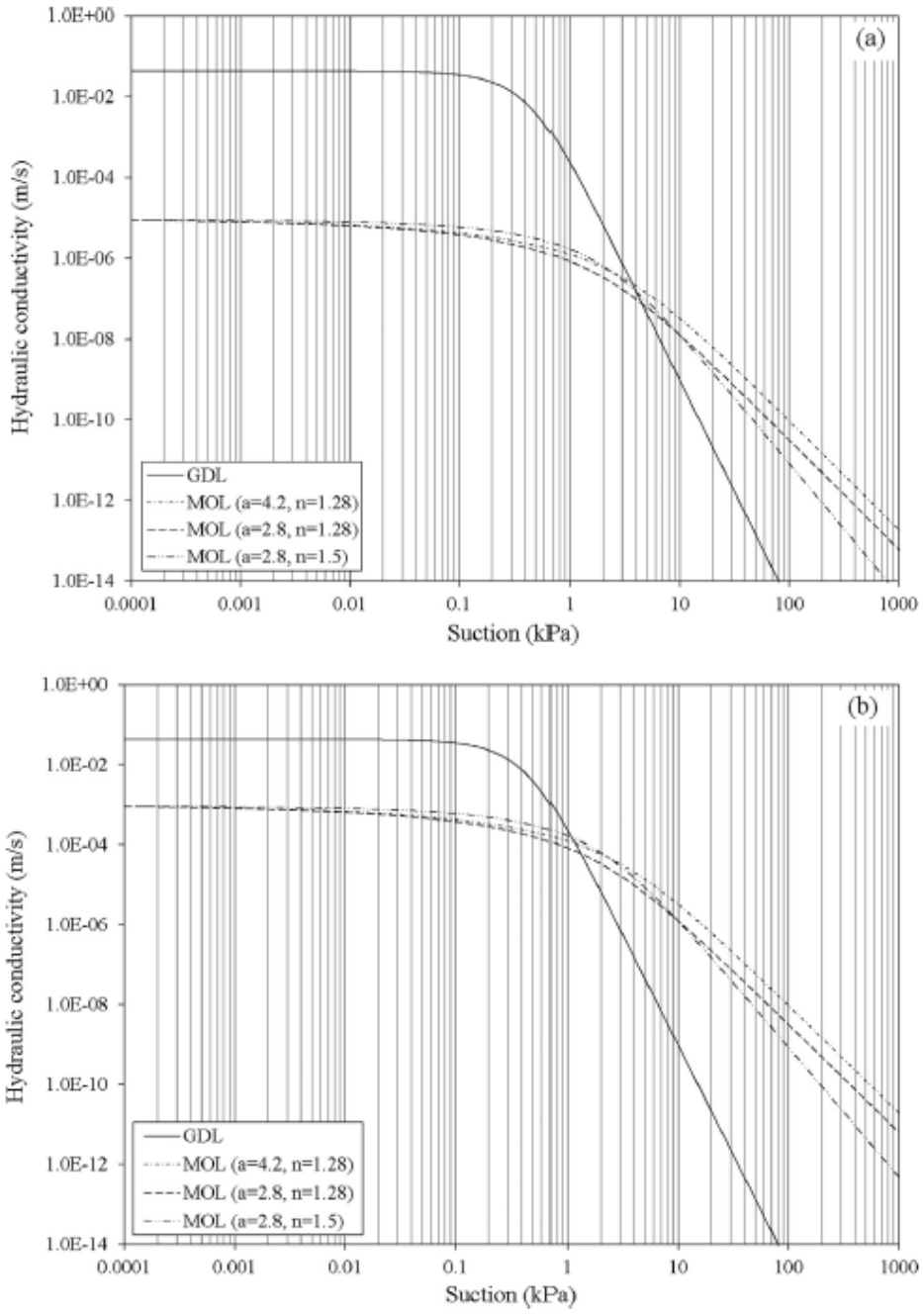

Figure 2: Hydraulic conductivity functions of the materials used in the parametric analysis; (a) $k_{sat\text{-}MOL} = 9\times10^{-6}$ m/s, and (b) $k_{sat\text{-}MOL} = 9\times10^{-4}$ m/s

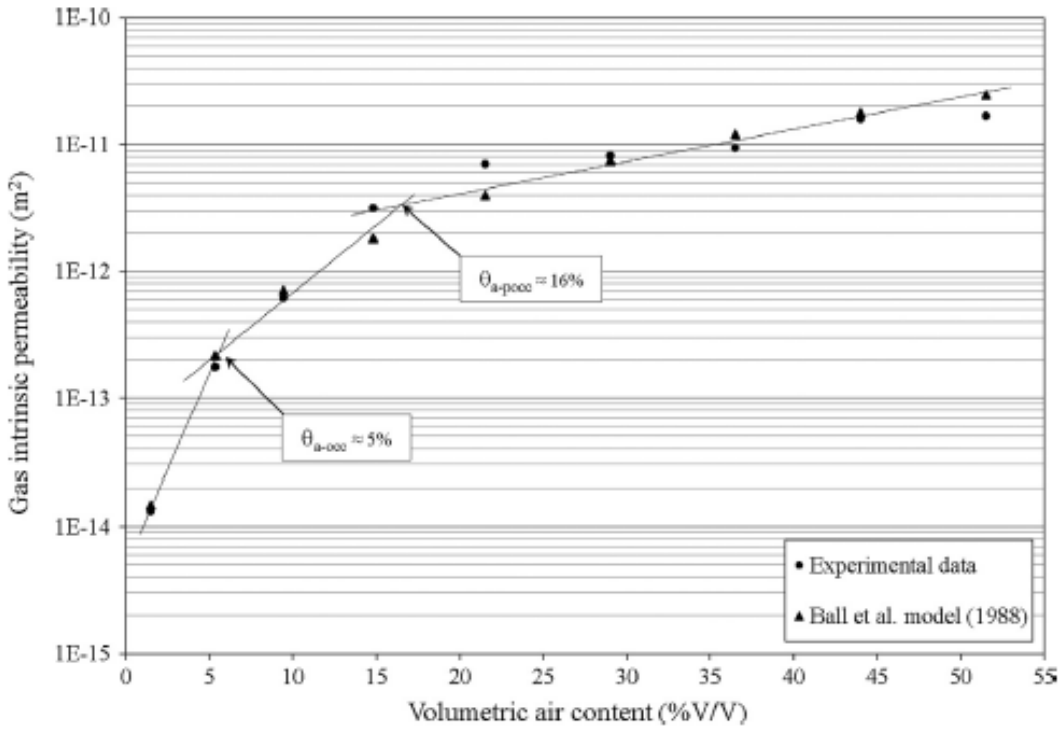

Figure 3: Gas intrinsic permeability function of the MOL material for numerical simulations with $k_{sat\text{-}MOL} = 9\times10^{-6}$ m/s

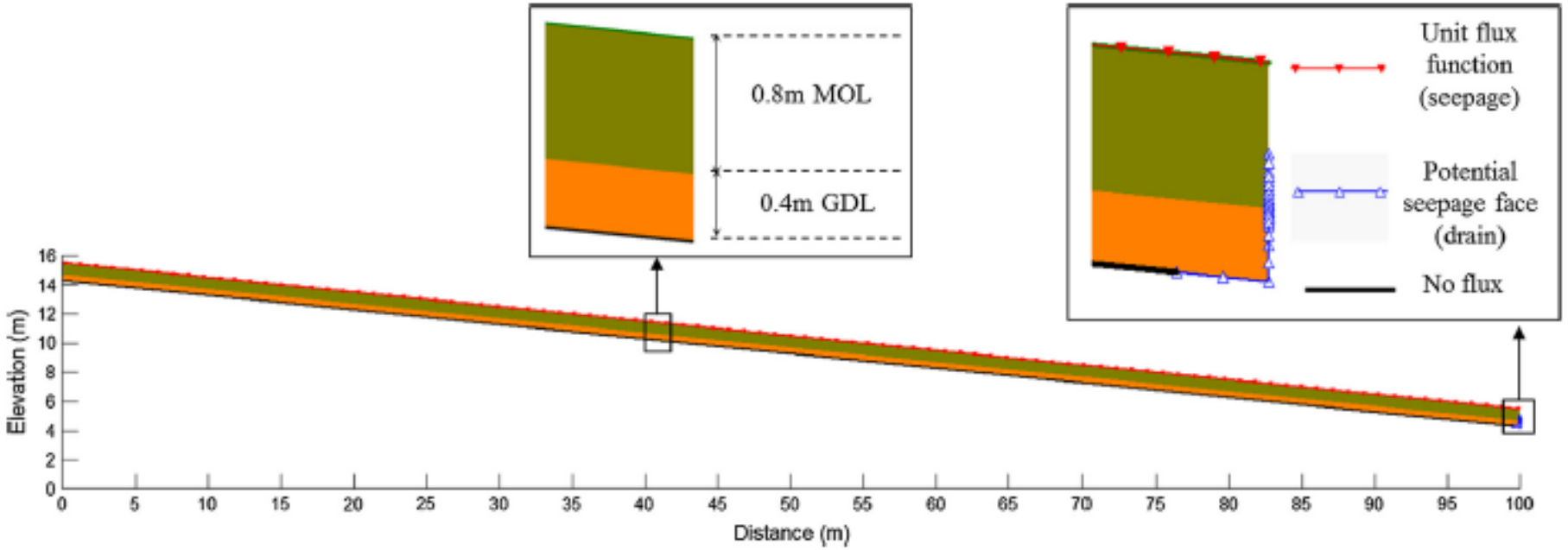

Figure 4: Dimensions and boundary conditions of the SEEP/W simulations (slope is variable)

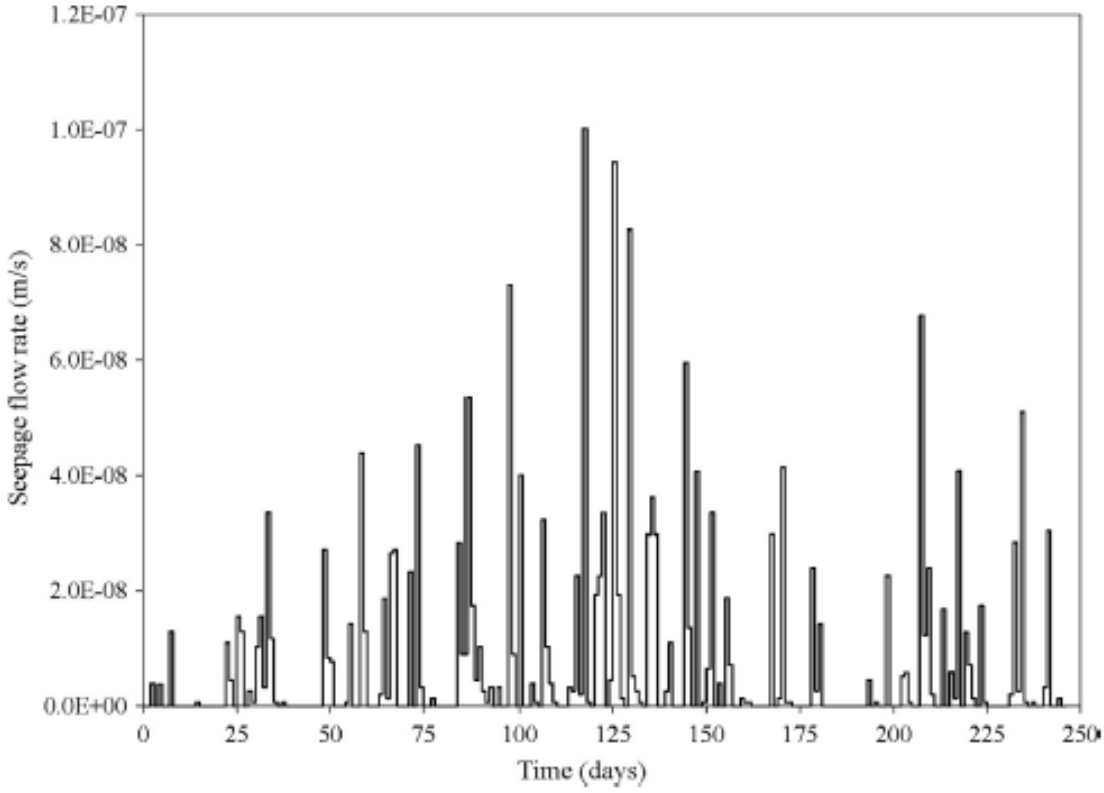

Figure 5: The daily rate of seepage into the PMOB2 during 246 days

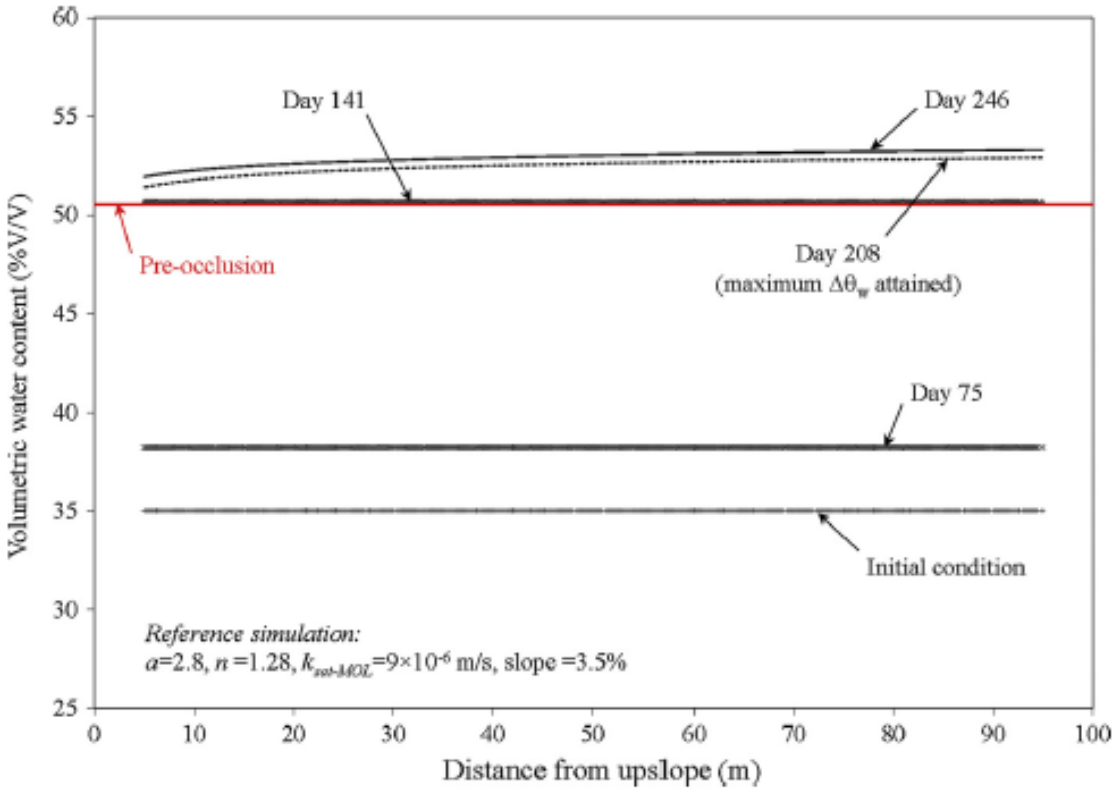

Figure 6: Distribution of θ_w in *interface points* at several time steps in simulation No. 1 (*Reference simulation*)

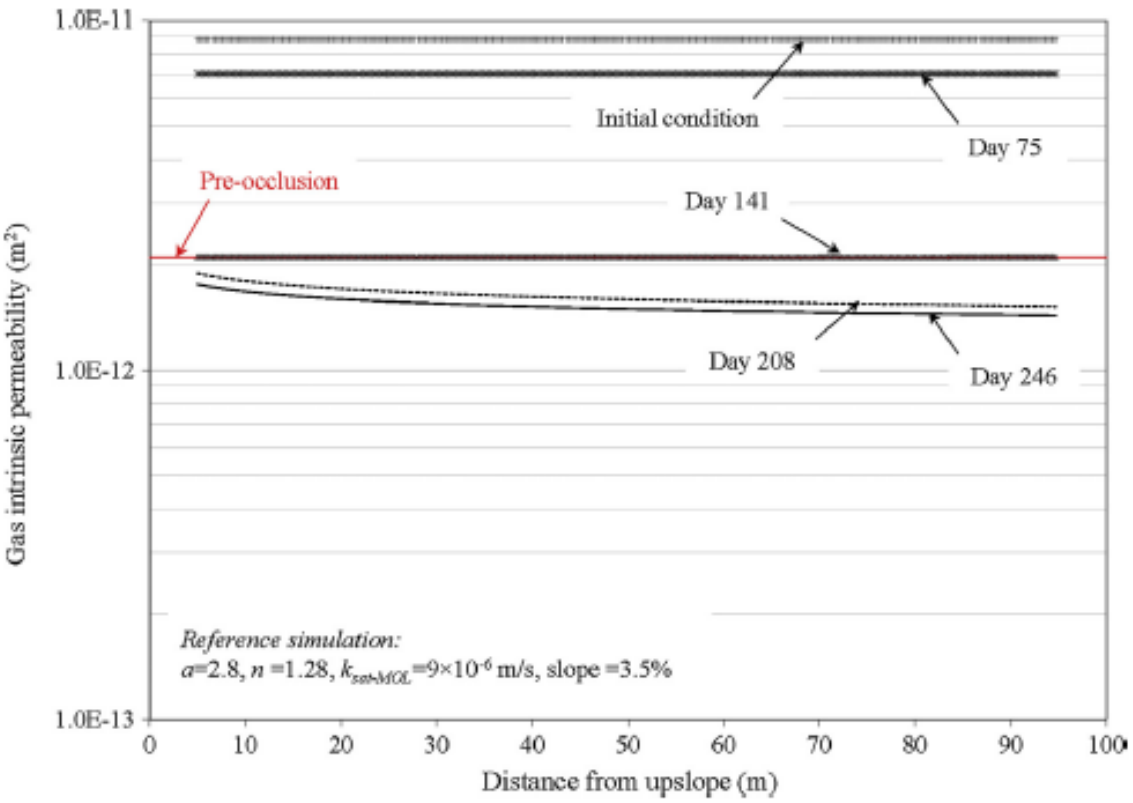

Figure 7: Distribution of K in *interface points* at several time steps, for simulation No. 1

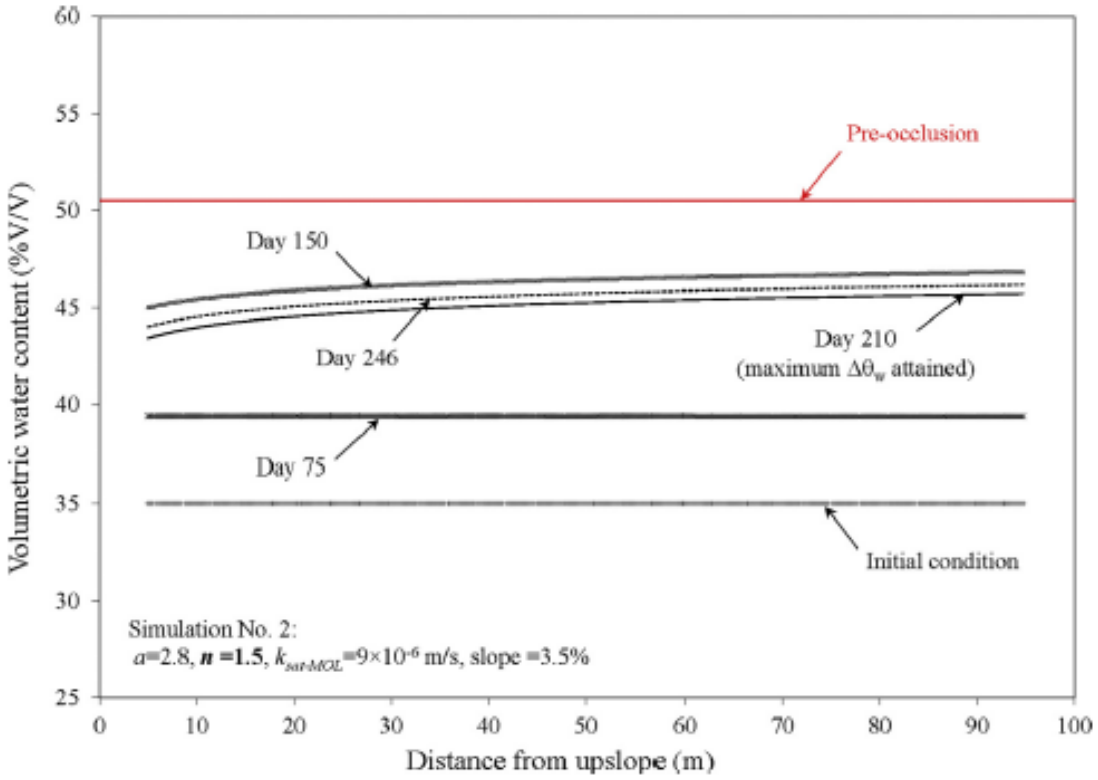

Figure 8: Distribution of θ_w in *interface points* at several time steps, for simulation No. 2

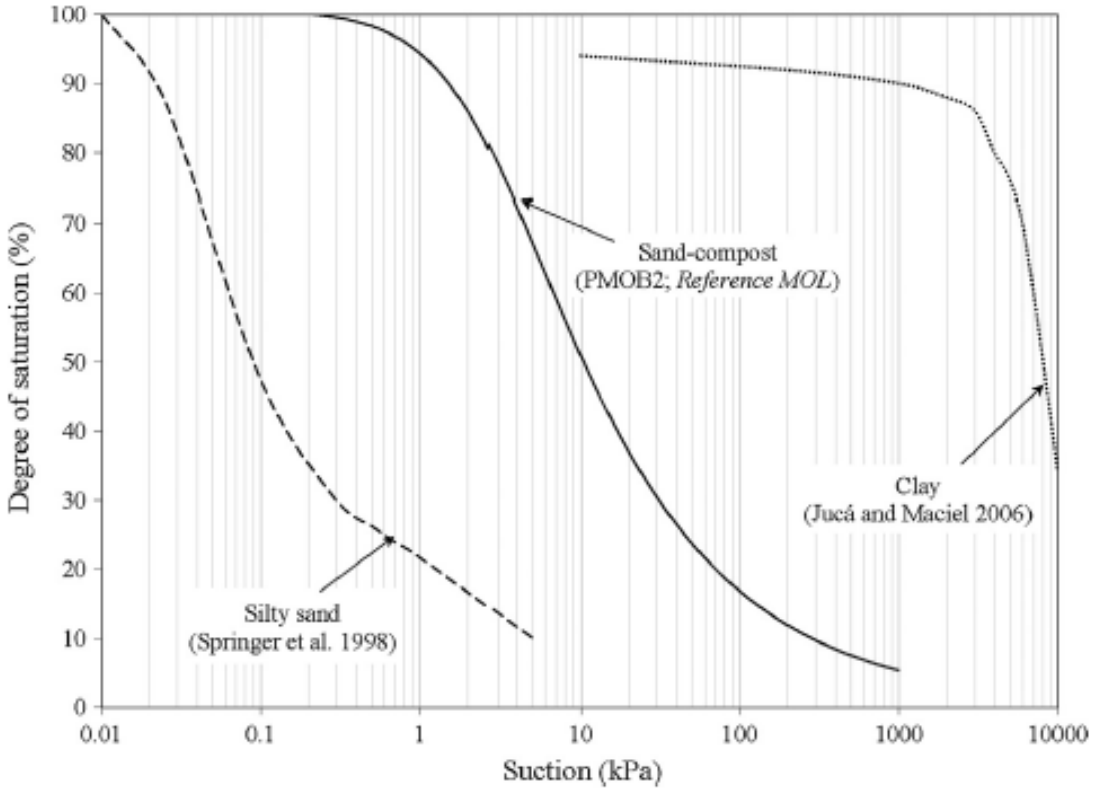

Figure 9: The water retention curve of the *Reference MOL* and materials from other studies (Jucá and Maciel 2006; Springer et al. 1998)

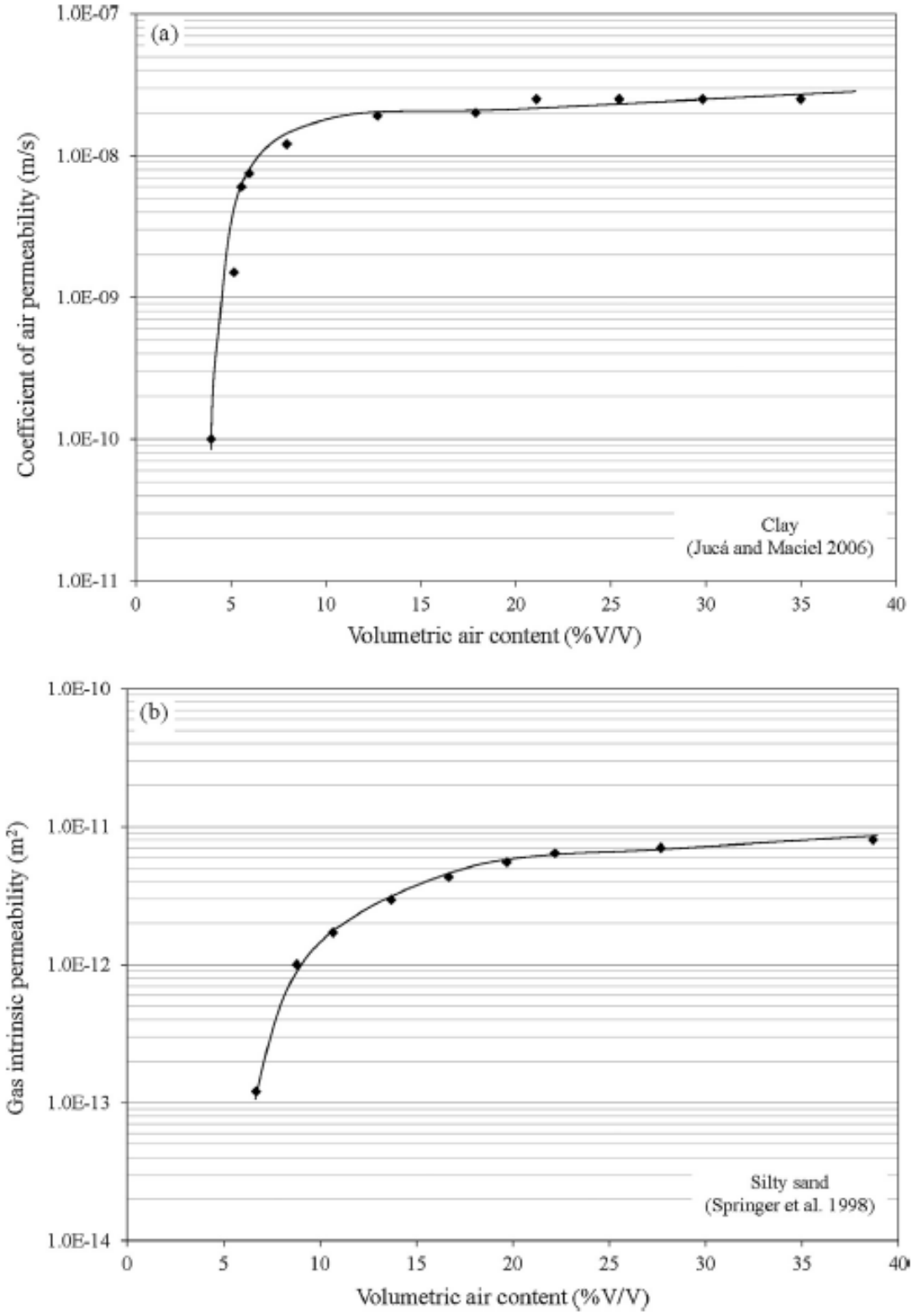

Figure 10: variation of (a) coefficient of air permeability and (b) gas intrinsic permeability with θ_a in materials from other studies (Jucá and Maciel 2006; Springer et al. 1998)

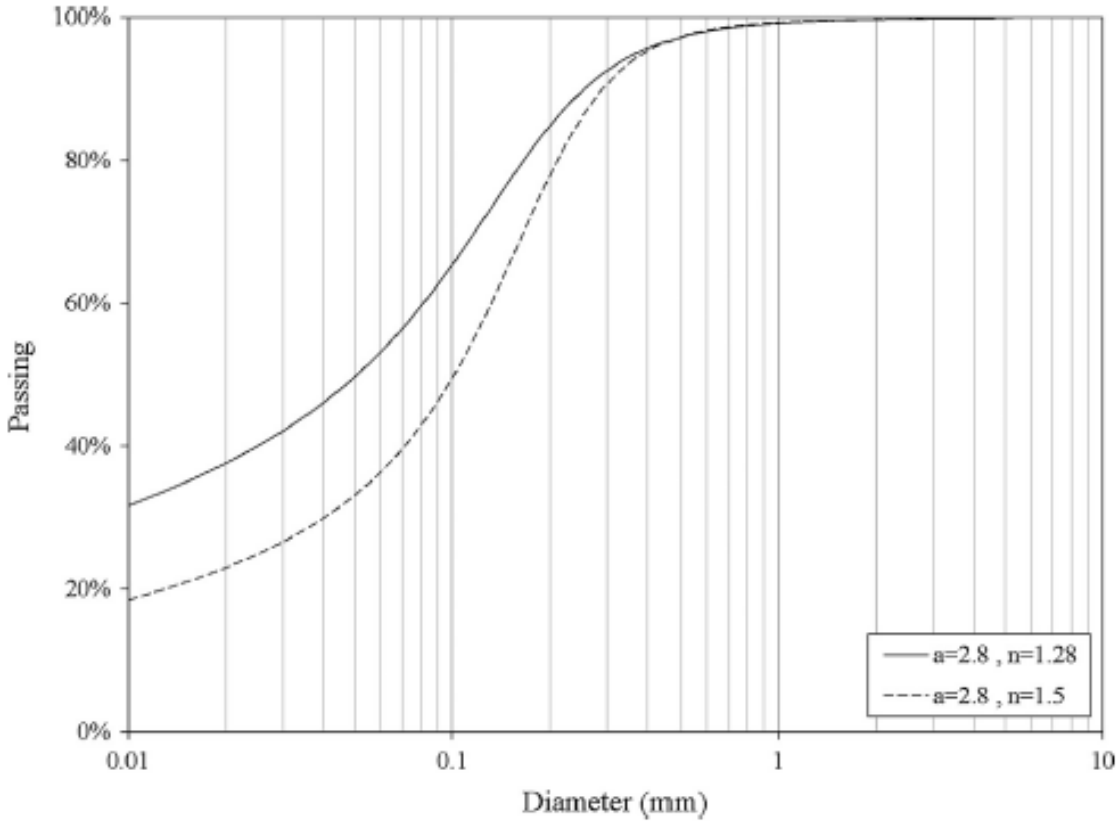

Figure 11: Corresponding grain size distribution curves of the water retention curves of the MOL materials for two cases (a=2.8 and n=1.28; a=2.8 and n=1.5), using the Fredlund et al. equation (2002)

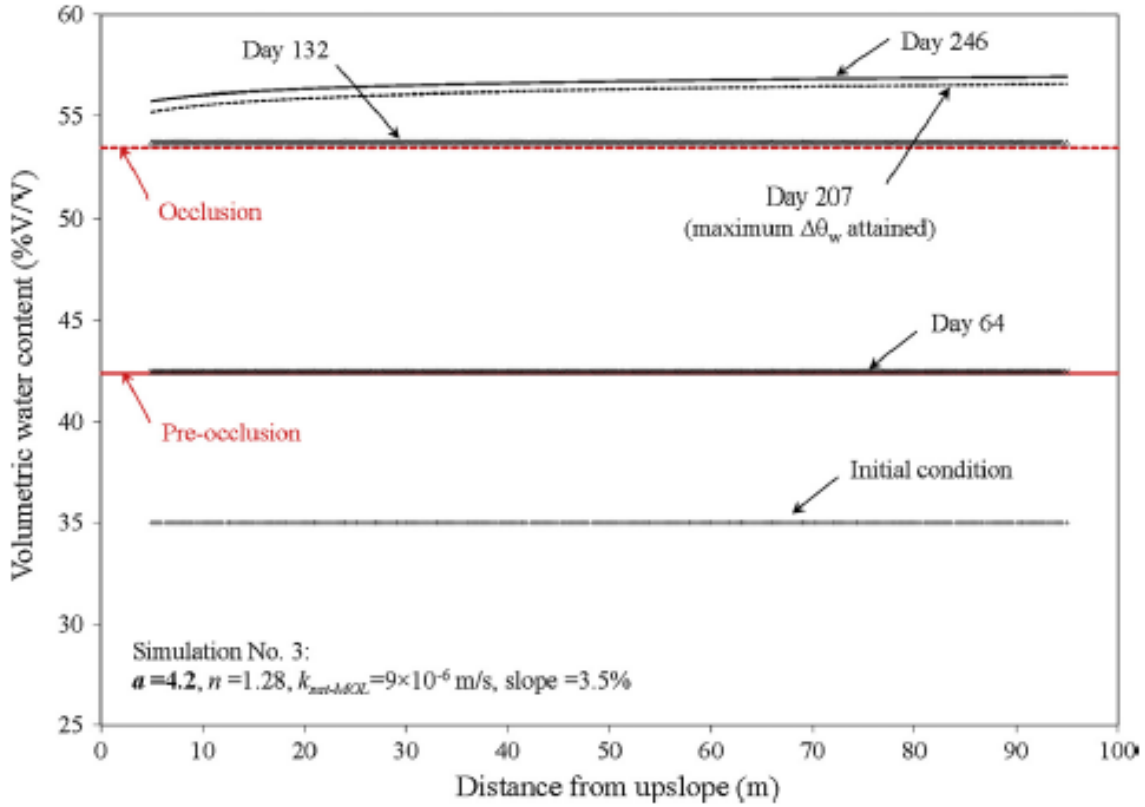

Figure 12: Distribution of θ_w in *interface points* at several time steps, for simulation No. 3

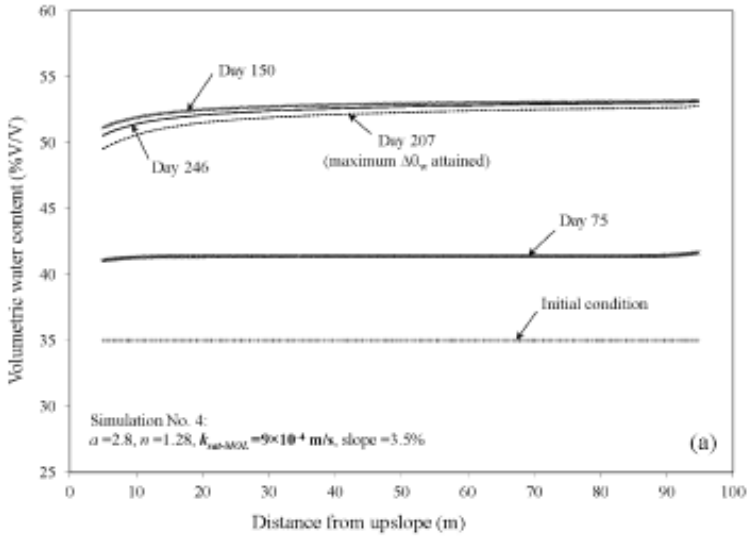

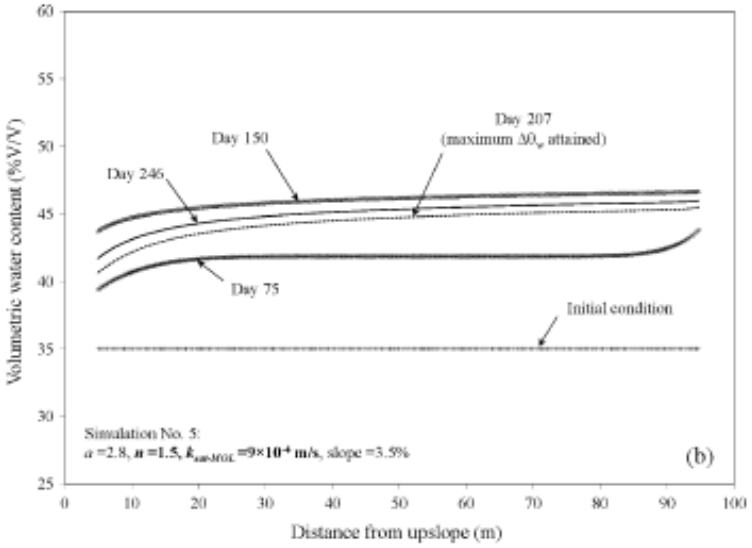

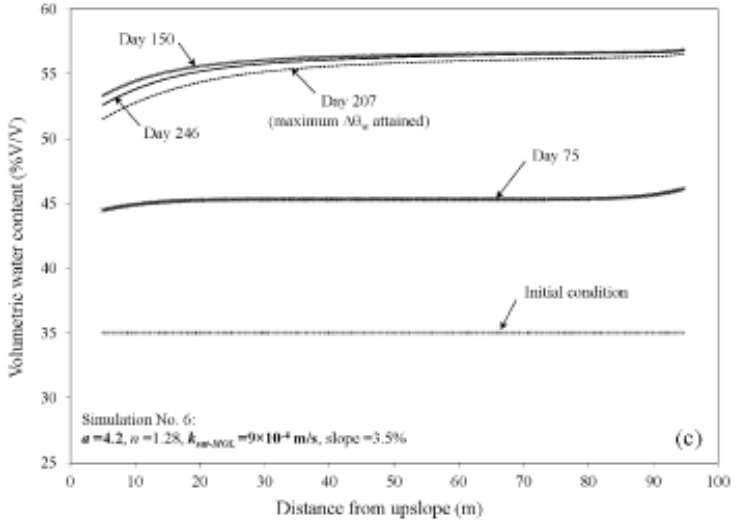

Figure 13: Distribution of θ_w in *interface points* at several time steps, for (a) simulation No. 4, (b) simulation No. 5, and (c) simulation No. 6

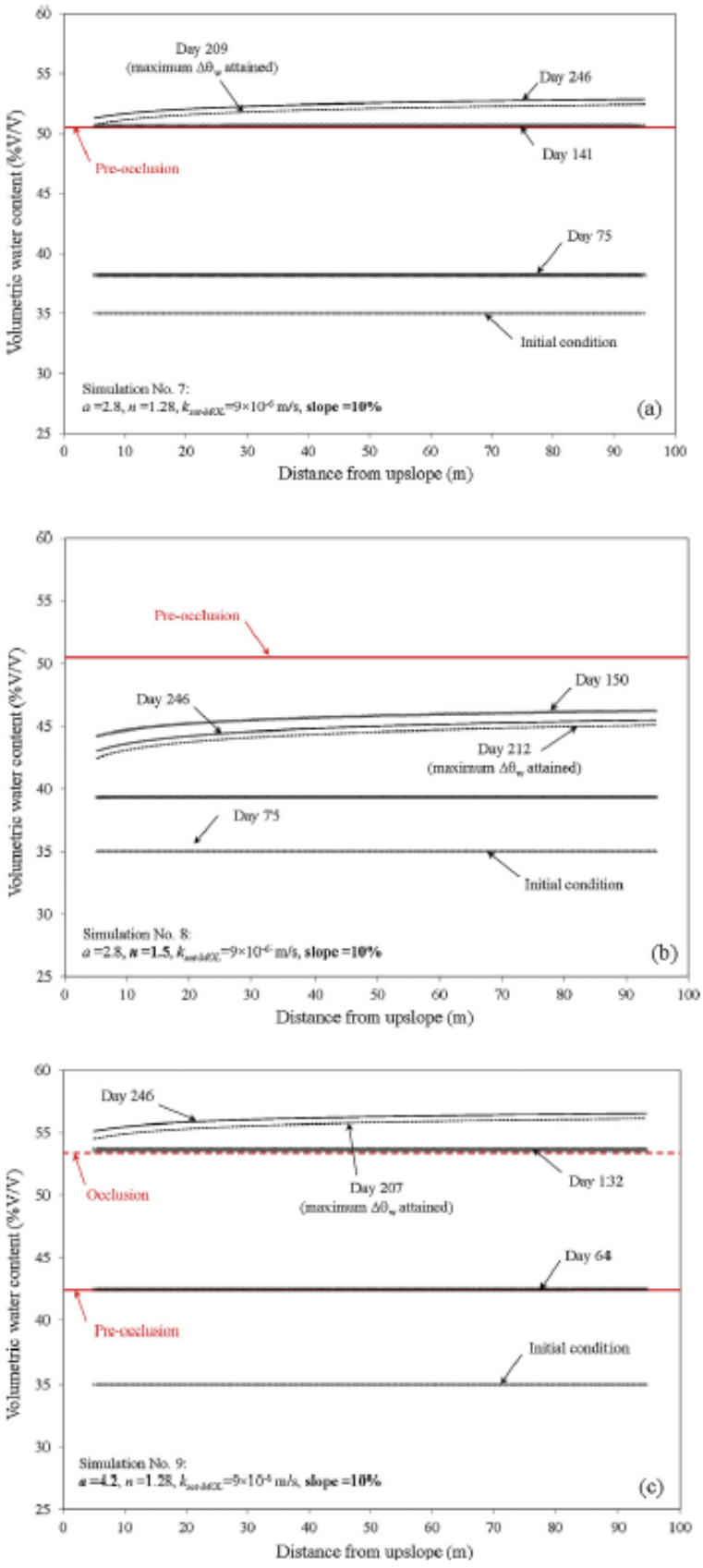

Figure 14: Distribution of θ_w in *interface points* at several time steps, for (a) simulation No. 7, (b) simulation No. 8, and (c) simulation No. 9

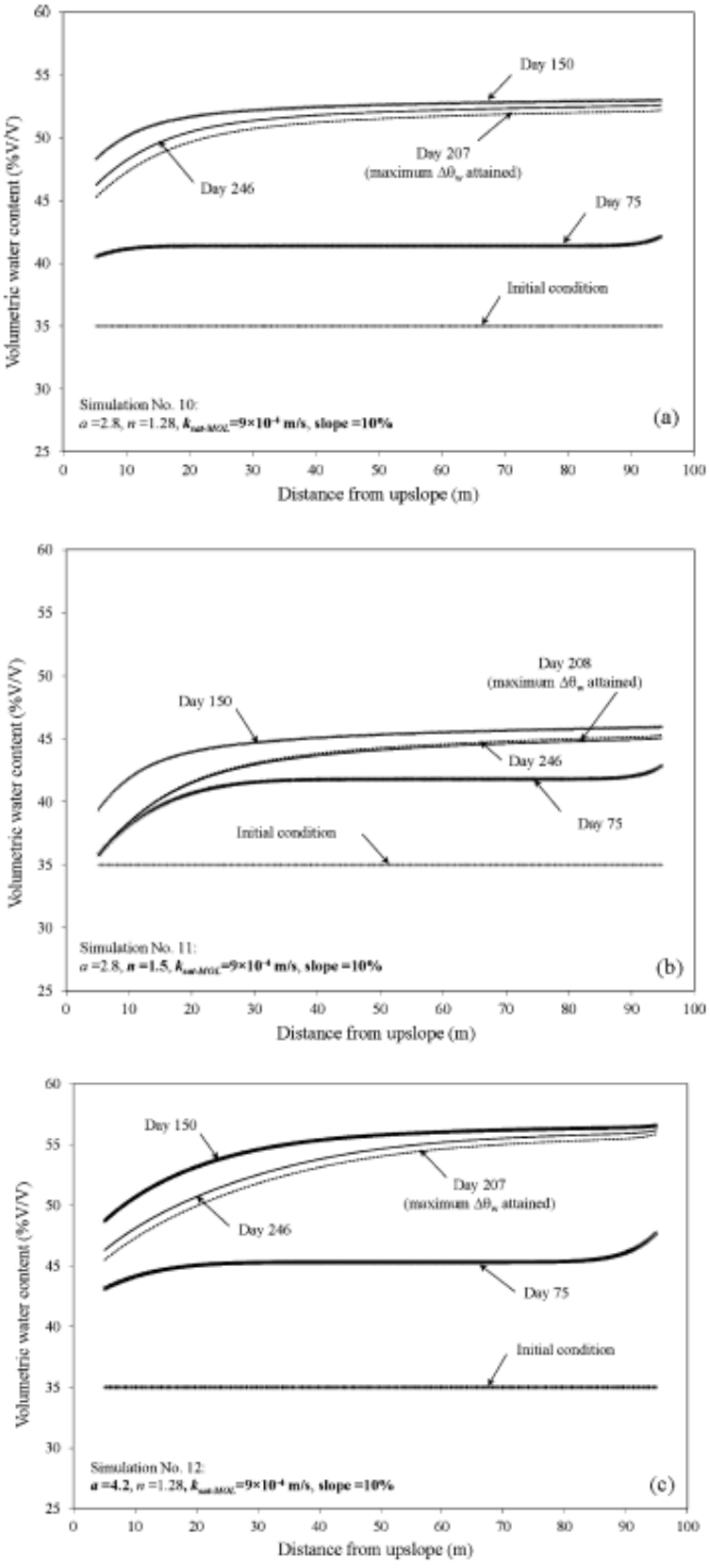

Figure 15: Distribution of θ_w in *interface points* at several time steps, for (a) simulation No. 10, (b) simulation No. 11, and (c) simulation No. 12

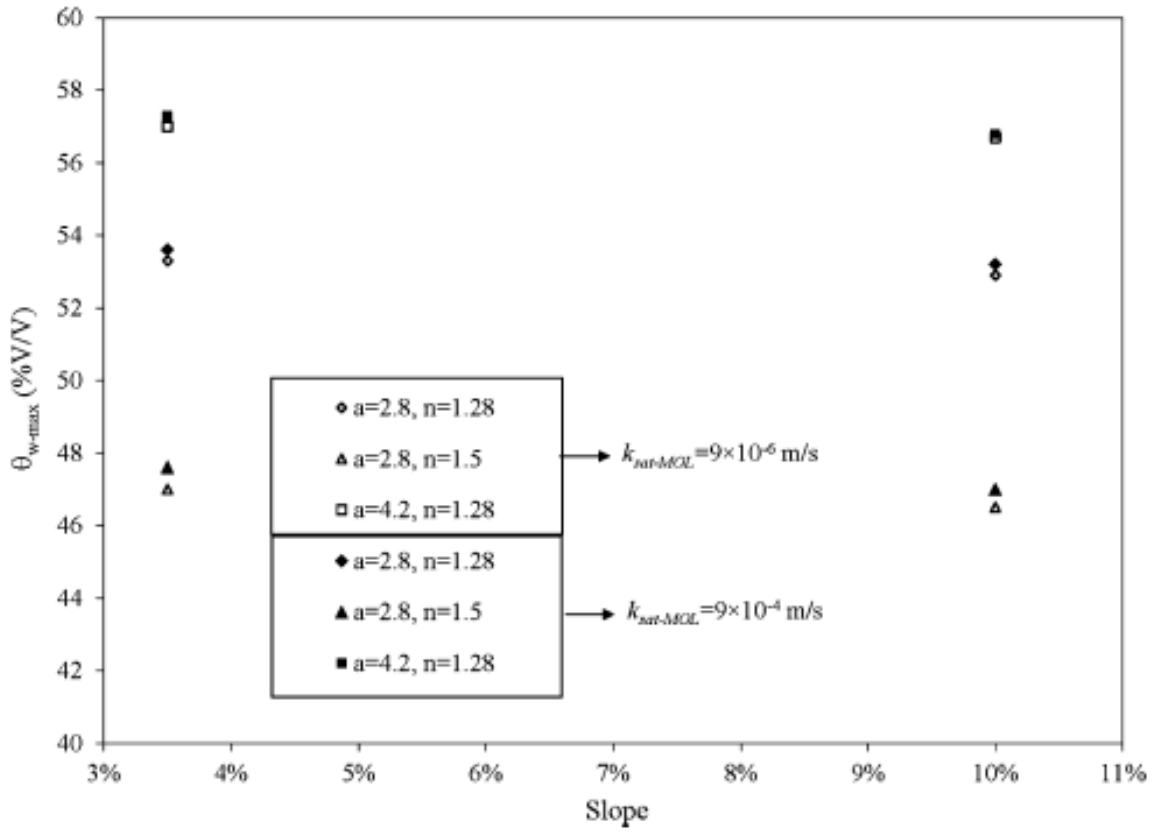

Figure 16: $\theta_{w\text{-}max}$ values in *interface points*, for several values of *a*, *n*, $k_{sat\text{-}MOL}$ and slope

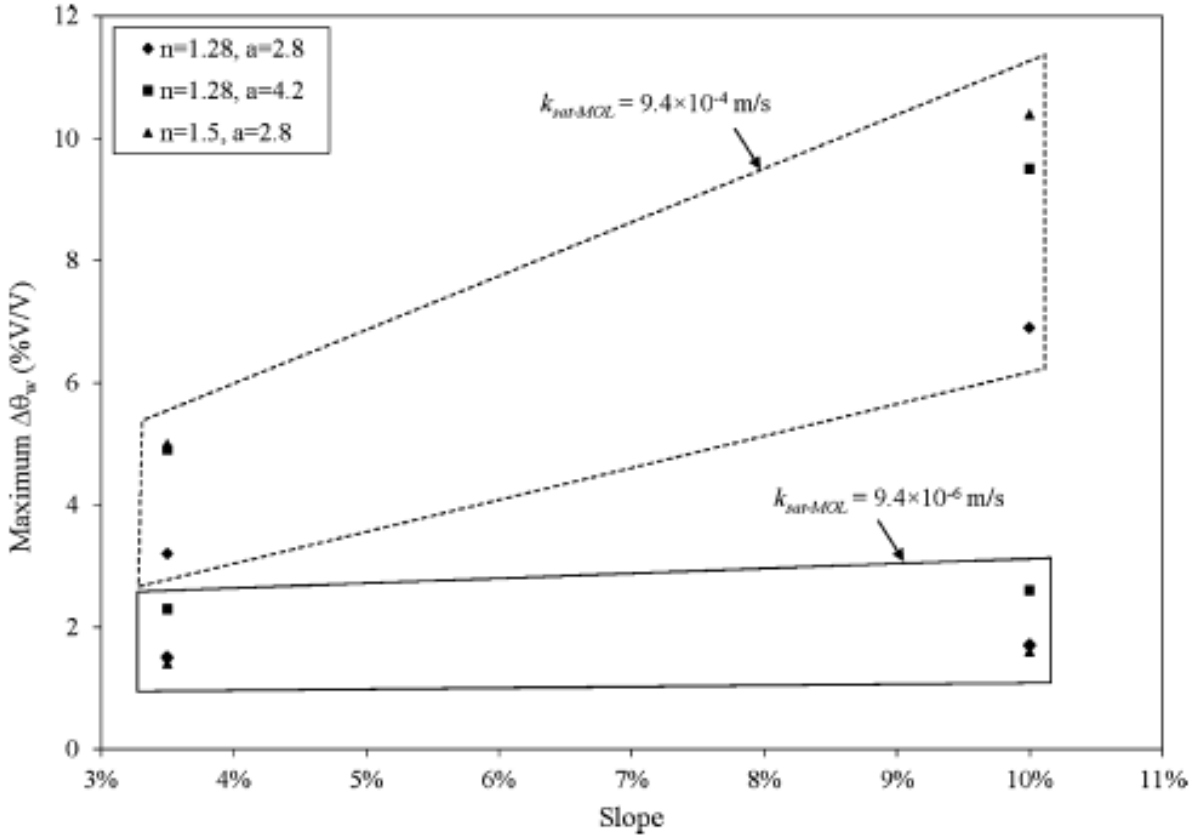

Figure 17: Maximum $\Delta\theta_w$ in *interface points*, for several values of a, n, $k_{sat\text{-}MOL}$ and slope

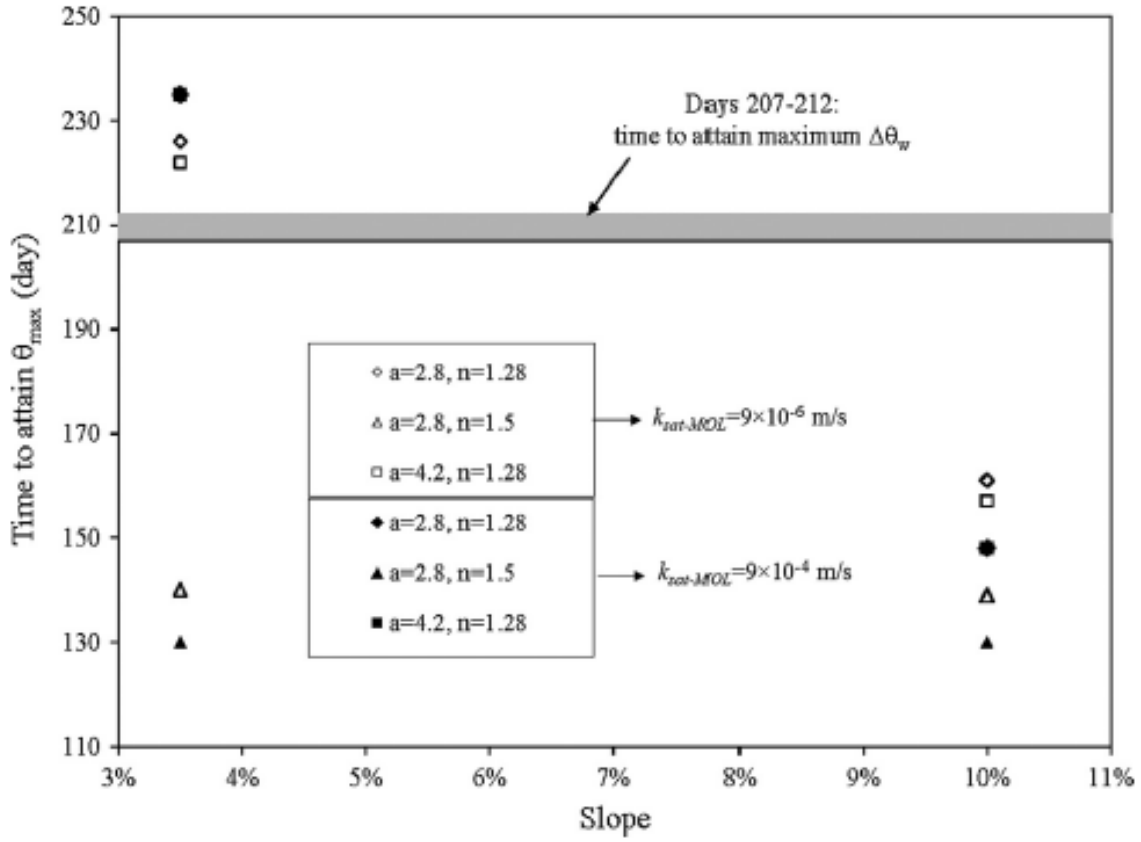

Figure 18: The time associated with attaining the $\theta_{w\text{-}max}$ in *interface points*, for several values of a, n, $k_{sat\text{-}MOL}$ and slope